



# Triaxial mechanical behaviours and life cycle assessment of sustainable multi-recycled aggregate concrete

Bin Lei<sup>a,b</sup>, Linjie Yu<sup>a</sup>, Yipu Guo<sup>b,\*</sup>, Hongjie Xue<sup>c</sup>, Xiaonan Wang<sup>b,e</sup>, Yan Zhang<sup>c</sup>, Wenkui Dong<sup>d</sup>, Frank Dehn<sup>f</sup>, Wengui Li<sup>b,f,\*</sup>

<sup>a</sup> School of Infrastructure Engineering, Nanchang University, Nanchang 330031, China

<sup>b</sup> Centre for Infrastructure Engineering and Safety, School of Civil and Environmental Engineering, The University of New South Wales, NSW 2052, Australia

<sup>c</sup> College of Harbour, Coastal and Offshore Engineering, Hohai University, Nanjing 210098, China

<sup>d</sup> Institute of Construction Materials, Technische Universität Dresden, 01062 Dresden, Germany

<sup>e</sup> School of Civil and Environmental Engineering, University of Technology Sydney, NSW 2007, Australia

<sup>f</sup> Institute for Concrete Structures and Building Materials, Karlsruhe Institute of Technology, 76131 Karlsruhe, Germany

## HIGHLIGHTS

- The triaxial failure modes of Multi-RAC is similar to conventional concrete.
- The multivariate regression mixed models properly estimate the triaxial mechanical properties.
- The Willam-Warnke failure criterion performs the best for Multi-RAC.
- An elastoplastic model was proposed with of recycling cycles into model's parameters.
- RACIII has the best compensation of 13.1 % carbon emission and 43.5 % energy consumption.

## GRAPHICAL ABSTRACT



## ARTICLE INFO

Editor: Ouyang Wei

### Keywords:

Multi-recycled aggregate concrete  
Triaxial behaviour  
Elastoplastic model

## ABSTRACT

Multi-recycling of concrete waste presents a promising avenue for carbon-negative development and a circular economy. This study comprehensively assesses the triaxial mechanical performance and environmental impact of multi-recycled concrete (Multi-RAC) through three recycling cycles. The results reveal a triaxial failure mode similar to natural aggregate concrete (NAC). The peak stress and peak strain monotonically increase with confinement stress, showing a significant impact (enlarged by 171.4 % to 280.6 % and 397.4 % to 412.0 %,

**Abbreviations:** AAE, Average absolute error; ANOVA, Analysis of variance; AP, Acidification potential; CED, Cumulative energy consumption; D-W, Durbin-Watson; EI, Environmental impact; EP, Eutrophication potential; GWP, Global warming potential; Multi-RA, Multi-recycled coarse aggregate; Multi-RAC, Multi-recycled aggregate concrete; IVs, Independent variables; LCA, Life cycle assessment; MSE, Mean square error; NA, Natural coarse aggregate; NAC, Natural aggregate concrete; ODP, Ozone layer depletion Potential; POCP, Photochemical ozone creation potential; RA, Recycled coarse aggregate; RAC, Recycled aggregate concrete; RACI, 1st generation of Multi-RAC; RACII, 2nd generation of Multi-RAC; RACIII, 3rd generation of Multi-RAC; RDV, Response dependent variable; SD, Standard deviation.

\* Corresponding authors at: Centre for Infrastructure Engineering and Safety, School of Civil and Environmental Engineering, The University of New South Wales, NSW 2052, Australia.

E-mail addresses: [yipu.guo-1@uts.edu.au](mailto:yipu.guo-1@uts.edu.au) (Y. Guo), [wengui.li@unsw.edu.au](mailto:wengui.li@unsw.edu.au) (W. Li).

<https://doi.org/10.1016/j.scitotenv.2024.171381>

Received 26 November 2023; Received in revised form 13 February 2024; Accepted 28 February 2024

Available online 3 March 2024

0048-9697/© 2024 The Authors. Published by Elsevier B.V. This is an open access article under the CC BY-NC-ND license (<http://creativecommons.org/licenses/by-nc-nd/4.0/>).

Failure criteria  
Life cycle assessment

respectively) from 0 to 20 MPa. All P-values for recycling cycles and confining pressure are less than 0.05, with the confining pressure having a more significant effect. Three best-fit multivariate mixed models predict mechanical properties, and a modified elastoplastic model introduces the recycling cycles factor. Numerical simulations confirm the model's accuracy in predicting the triaxial mechanical properties of Multi-RAC. Comparative analysis reveals that the elastoplastic model-derived non-integral high order failure criterion outperforms the Willam-Warnke failure criterion and other conventional criteria. Regarding environmental impact, all indicators (GWP, POCP, AP, EP, and CED) decrease favourably with the increasing number of recycling cycles, with CED and EP playing the most significant roles. Compared to NAC, the five environmentally favorable indicators for RACIII decrease by 3.24 % to 50.6 %, respectively. These findings provide valuable insights for future research on developing eco-friendlier Multi-RAC for sustainable and green infrastructure.

## 1. Introduction

The rapid development of infrastructure and industrial construction has led to an increasing demand for concrete materials (Tang et al., 2020; Lu, 2019). Waste concrete is also the main construction waste generated during the demolition of various obsolete buildings, which can cause a heavy burden on the environment and landfills (Dey et al., 2022; Xiao et al., 2022a). Recycling waste concrete into recycled building materials such as recycled aggregates and recycled concrete through a series of shredding processes is regarded as a more sustainable, viable, and practical solution to deal with the enormous amount of concrete waste, especially compared to landfilling (Kisku et al., 2017). Therefore, intensive efforts have been placed on the research of recycled aggregate concrete (RAC), including macro-property influencing factors (recycled coarse aggregate replacement ratio, quality, etc.) (Gonçalves et al., 2020; Li et al., 2018; Ma et al., 2020), micro-interfacial characteristics (interfacial transition zone thickness, micromechanical properties, etc.) (Bahraq et al., 2022), and modification methods of recycled aggregates (acid solutions, surface layer, etc.) (Huang et al., 2021).

Over the past decades or so, there has been increasing research interest on the multi-recycling of concrete, which promotes the sustainable development. The concept of multi-recycling is to repeatedly recycle coarse aggregate by crushing the last generation of concrete waste, which is used to replace natural aggregate in manufacturing the next generation of multi-recycled coarse aggregate (Multi-RA). Owing to the susceptible attributes to the damage involved in the complex shredding processes during the multi-recycling and the inconsistent quality and age of each generation of Multi-RA, Multi-RAC often presents inconsistent performance (Lei et al., 2023a). The current research status of Multi-RA and Multi-RAC mainly focuses on their material properties in the fresh and hardened states, including mechanical (Huda and Alam, 2014; Kim et al., 2023), microstructural (Thomas et al., 2020; Thomas et al., 2018), and durable properties (Liu et al., 2022; Silva et al., 2021). Specifically, most studies investigated the mechanical properties under a simple uniaxial stress state, including peak strain (Chen et al., 2019a), peak stress (Chen et al., 2022), compressive strength (Salesa et al., 2017), dynamic compression strength (Xiao et al., 2015), splitting tensile strength (Zhu et al., 2016).

In addition to the research on RAC performance, scholars have gradually realized the importance of the environmental impact of recycled concrete. Xiao et al. (Xiao et al., 2022b) evaluated the life cycle environmental benefits of RAC based on life cycle assessment (LCA) and they found that the carbon emission factor of RA was 7.1 % lower than natural coarse aggregate (NA), and the life cycle carbon emission of RAC was 15 kg CO<sub>2</sub>eq/m<sup>3</sup> lower than NAC. Moraes et al. (Borges et al., 2023) found that recycled aggregates with particle size below 2.4 mm can absorb 63 % of the carbon emissions from the production phase of RAC when they completely replace natural aggregates. In addition, Mazurana et al. (Mazurana et al., 2021) have again demonstrated that RA has a great potential for carbon reduction. Specifically, a life cycle environmental benefit analysis of RAC found that RAC can capture 165.34 kg CO<sub>2</sub>eq/ m<sup>3</sup> over its full life cycle, while NAC only captures 53.4 kg CO<sub>2</sub>eq/ m<sup>3</sup>.

Nevertheless, in-service concrete structures often experience

complex triaxial loading. Few studies have performed the experimental analysis of RAC subjected to confining triaxial compression and true triaxial compression. Folino and Xargay (Folino and Xargay, 2014) investigated the triaxial mechanical behaviour of RAC with the replacement ratios of 30 %, 60 %, and 100 %. The compressive failure meridian shows a nonlinear correlation with the increasing confining pressure, while no obvious discrepancy in failure mode was captured for RAC with different replacement ratios. Chen et al. (Chen et al., 2019a) reported that the RA replacement ratio merely affected the shape of triaxial constructive curves of RAC, whereas the shape was significantly influenced by the later confinement. It is worth noting although some conventional models involving Mohr-Coulomb model (Chen et al., 2019a), Willam-Warnke model (Wu et al., 2023), Drucker-Prager model (Li et al., 2022), and concrete damage plasticity model (Li et al., 2022) were proposed to describe the failure stress evolution under the confining compressive loading condition, the strain characteristics cannot be presented by failure criterion. Although few empirical models were proposed by scholars to describe the triaxial constructive curve for RAC (Chen et al., 2019a; Chen et al., 2023), these empirical models were unable to capture the plastic strain from the deformation characteristics, attributing to the lack of plastic criteria and flow rate. Overall, the experimental and analytical research on triaxial mechanical properties and the corresponding failure criteria are very limited, let alone the Multi-RAC. Meanwhile, there is the absence of LCA studies for Multi-RAC. In this context, this study aims to comprehensively investigate the triaxial mechanical performance and environmental impact of Multi-RAC. The differences in NAC and three generations of Multi-RAC are compared. Three conventional failure criteria (Mohr-Coulomb, Power-law, and Willam-Warnke) and a non-integer high order failure criterion derived from a modified elastoplastic model were proposed, and their performance was evaluated. The related outcomes and insights are expected to serve as valuable sources for future investigations into developing eco-friendlier Multi-RAC as structural concrete (Dong et al., 2019; Ke et al., 2023; Li et al., 2024; Wang et al., 2024).

## 2. Experimental program

### 2.1. Raw materials

The crushed basalt provided by the local quarry (Nanchang, China) served as natural coarse aggregate (NA). Natural river sand (fineness modulus of 2.8, medium coarse sand) served as fine aggregate. Ordinary Portland cement (PO. 42.5) served as the binder, and the physical and mechanical properties as shown in Table 1. A naphthalene-based water-

**Table 1**  
Physical and mechanical properties of cement.

Consistency (%)	Specific surface area (m <sup>2</sup> /kg)	Compressive strength (MPa)		Flexural strength (MPa)		Setting time (min)	
		3-day	28-day	3-day	28-day	Initial	Final
0.3	359	28.6	57.3	6.1	9.3	202	237

reducing agent served as the water reducer. Laboratory tap water was used throughout the experiment.

## 2.2. Specimen preparation

The preparation procedure to obtain three generations of Multi-RCA, namely RAI, RAII, and RAIII, is described as follows. NCA at the age of 28 days was crushed in the laboratory by a jaw crusher and subsequently screened and cleaned to obtain the RAI. The RAI was used to 100 % replace the NA to manufacture the 1<sup>st</sup> generation of Multi-RAC (RACI) (Fig. 1 (a)). An identical working route was applied to prepare 2<sup>nd</sup> and 3<sup>rd</sup> generations of Multi-RAC (RACII, RACIII) shown in Fig. 1 (b). To minimize the interruptions from the age of parent concrete on the quality of the recycled aggregates, all generations of Multi-RA were obtained from the last generations of Multi-RAC at the age of 28 days. The gradations of RAI, RAII, and RAIII were kept identical to NAC by means of being sieved and separated by size fraction (Zhu et al., 2019) and met the requirement of Chinese standard JGJ 52-2006 (*Standard for Technical Requirements and Test Method of Sand and Crushed Stone (or Gravel) for Ordinary Concrete (JGJ 52-2006)*, 2006) in Fig. 1 (c). The physical indexes of four groups of specimens are listed in Table 2, which were measured in accordance with Chinese standard GB/T25177-2012 (*Recycled Aggregate for Concrete (GB/T25177-2012)*, 2014). Previous studies agreed that the volume fraction of NA in Multi-RAC significantly and incrementally decreases with the increasing number of recycling cycles (Lei et al., 2023a; Xiao et al., 2007). It is experimentally verified that the volume fraction of adhered old mortar can make up more than 80 % of the total volume of Multi-RA after 3 recycling cycles, which is a vital factor in compromising the mechanical properties of the resultant concrete (Thomas et al., 2020; Thomas et al., 2018). The content of attached mortar was evaluated based on the method presented in Ref. (De Juan and Gutiérrez, 2009), which evidently increased as the number of recycling cycles increased.

The mix design of NAC and three generation of Multi-RAC refers to the requirement of JGJ 55-2011 (*Specification for Mix Proportion Design of Ordinary Concrete (JGJ 55-2011)*, 2011), as shown in Table 3. All generations of Multi-RAC were prepared by presaturation method to maintain the effective water-to-cement (w/c) ratio (Lei et al., 2020; Lei et al., 2018). The mixing procedure was detailed in Ref. (Lei et al., 2023b). The 50 × 100 mm cylindrical specimens were prepared. The samples covered by plastic film and initially cured for 2 days. Then they were demolded and cured in a saturated calcium hydroxide solution for 26 days to ensure the minimization of adverse effects due to temperature and humidity changes and calcium hydroxide precipitation within the concrete.

## 2.3. Testing methods

### 2.3.1. Triaxial confinement compression

The testing equipment was GCTS RTX-4000 high-pressure and high-temperature triaxial rock testing system shown in Fig. 1 (d). The axial and radial deformations will be measured using linear variable differential transducers (LVDTs). The radial LVDT was placed at canter section of the specimen to minimize the end friction effects. The loading path was constructed by two stages illustrated in Fig. 1 (e). In the initial stage, the axial deviatoric pressure and confining pressure were loaded at a rate of 0.2 MPa/s using the force control mode to the target values 5, 10, 15, and 20 MPa. In the following stage, the axial deviatoric pressure was loaded at a 0.1 mm/min rate until failure occurred.

### 2.3.2. Life cycle assessment

**2.3.2.1. Scope and boundary.** The goals of this study are: (i) to evaluate the environmental benefits of Multi-RAC with different RA recycling numbers in comparison to conventional NAC; (ii) to predict the relative

contributions of energy consumption and carbon emission environmental impact (EI) indicators in different life cycle stages for four generations concrete. Previous studies have demonstrated that the environmental impact of NAC and RAC structures are expected to be similar under non-aggressive ambient conditions during the construction, in-service, and demolition stages (Ding et al., 2016). Additionally, recycling waste concrete to prepare recycled aggregates avoids the potential negative environmental impacts of direct landfilling (Xiao et al., 2018). Therefore, this study included the EI of the post-demolition treatment stage of concrete construction into the system boundary, focusing on comparing the relative EI of NAC and three generations Multi-RAC, rather than the absolute EI.

Along these lines, based on 'cradle-to-cradle' LCA, this study divides the life cycle of NAC and three generations Multi-RAC into raw material extraction and transportation, concrete preparation and transportation, concrete construction and demolition, and waste concrete post-demolition treatment stages. Although the EI of concrete buildings in the operation stage can account for 80 % ~ 90 % of the whole life cycle (Wang et al., 2008), the variability of the EI for NAC and three generations of Multi-RAC buildings during the operational stage is still not taken into account, mainly because NAC and RAC have the same EI during the construction and operational stages (Knoeri et al., 2013; Wu et al., 2012). Fig. 2 depicts the system boundary of NAC and three generations of Multi-RAC based on 'cradle-to-cradle' LCA.

**2.3.2.2. Life cycle inventory.** The material life cycle assessment method, CML 2001 - Jan. 2001 (baseline), was studied to assess the EI of traditional NAC, RACI, RACII, and RACIII. Six EI categories, including Global Warming Potential (GWP), Ozone Layer Depletion Potential (ODP), Photochemical Ozone Creation Potential (POCP), Acidification Potential (AP), Eutrophication Potential (EP) and Cumulative Energy Consumption (CED) were selected, wherein the CED involves consumption of primary energy, either renewable or non-renewable (Braga et al., 2017).

The life cycle inventory (LCI) of raw materials extraction and transportation, and concrete preparation and transportation for NAC and three generations Multi-RAC was shown in Tables S1 and S2, respectively. The EI of the concrete construction stage is twice that of concrete the transportation stage, and the EI of concrete buildings demolition stage is 90% of that of the concrete construction stage, which is consistent with Gong et al. (Gong et al., 2012). The LCI of concrete construction and demolition, and waste concrete post-demolition treatment stages are shown in Table 4.

## 3. Results and discussions

### 3.1. Failure mode

The failure modes of NAC and three generations of Multi-RAC are illustrated in Fig. 3. When under uniaxial compression, four groups of specimens show the characteristics of brittle failure. The failure process was divided into three stages of crack initiation, crack extension, and specimen failure. When the load approaches the peak stress, no obvious cracks are captured. After loading to the peak stress, all four groups of specimens formed microcracks and finally converged into penetrating main cracks parallel to the axial direction. However, the number of transverse cracks seems to appear as the number of recycling cycles increases, which is probably owing to the fact certain initial damage is accumulated during the multi-recycling process and a more pronounced radial crack expansion phenomenon is presented in Multi-RAC with increasing number of recycling cycles (Lei et al., 2023c).

When under the triaxial confining compression, all groups of the specimens presented oblique shear failure with the presence of diagonal shear cracks and good integrity, which shows a good agreement with other cement-based composites subjected to triaxial compression (Chen et al., 2023; Yang et al., 2022). In particular, it seems that the width of

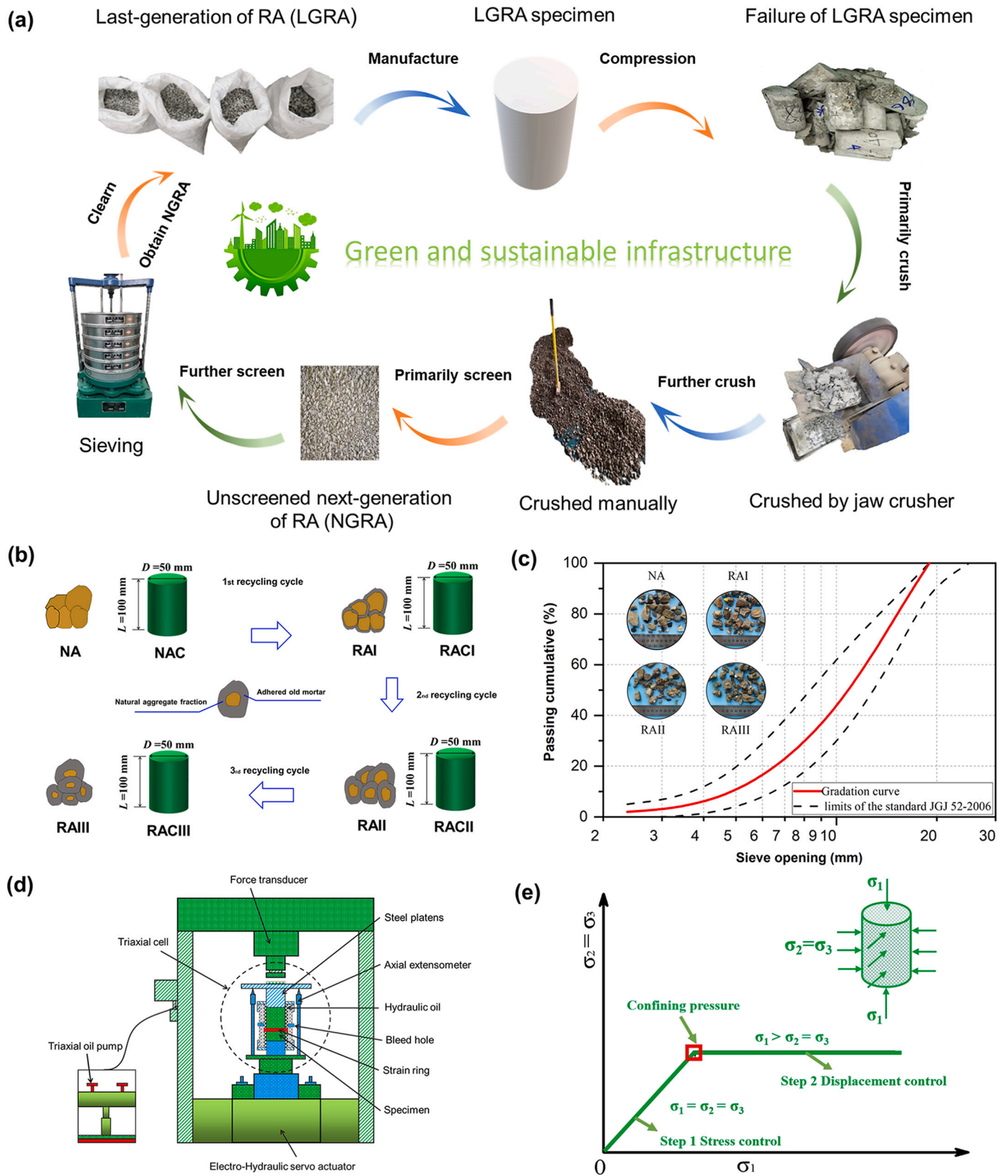


Fig. 1. Triaxial mechanical test on Multi-RAC: (a) Working route of recycling cycles; (b) Three generations of Multi-RAC; (c) Gradation curve, (d) Triaxial testing system, and (e) Loading regime.

**Table 2**  
Physical indexes of four groups of specimens.

Groups	Grading (mm)	Crush indicator (%)	Apparent density(kg/m <sup>3</sup> )	Water absorption(by mass %)	Void ratio (%)	Adhered mortar (by mass %)
NA	5–20	11.63	2828	1.1	45.7	0
RAI	5–20	14.79	2746	5.7	49.5	5.9
RAII	5–20	16.10	2728	8.4	52.2	8.7
RAIII	5–20	18.07	2710	9.7	53.3	9.8

**Table 3**  
Mix design of four groups of specimens.

Groups	Water (kg/m <sup>3</sup> )	Cement (kg/m <sup>3</sup> )	Sand (kg/m <sup>3</sup> )	Aggregate (kg/m <sup>3</sup> )	Water reducer (kg/m <sup>3</sup> )	28-day cubic compressive
NAC	195	527	630	1074	2.635	50.3
RACI	195	527	619	1054	2.635	48.5
RACII	195	527	617	1050	2.635	47.2
RACIII	195	527	614	1046	2.635	45.3

diagonal cracks is smaller for Multi-RAC compared to the conventional NAC, especially at higher confining pressure and later generation. The transverse constraint forces will make the attached old mortar of Multi-RAC continuously fill the internal micropores and fine cracks and enhance the bond between aggregate and cement matrix. Multi-recycled coarse aggregate is essentially comprised of the natural aggregate portion and attached old mortar portion, while the stiffness and strength of both portions decrease as the number of recycling cycles reduces, making the concrete less susceptible to the formation of penetration cracks (Chiaia et al., 1998; Akçaoğlu, 2017). Overall, the results indicate

the failure modes of Multi-RAC specimens are similar to the conventional NAC. The failure mode is significantly affected by the confining pressure, whereas it is insignificant affected by the recycling cycles.

3.2. Mechanical behaviours

According to the experimental results, Table 5 lists the average values of the uniaxial compressive strength ( $f_{co}$ ), confining stress ( $\sigma_w$ ), confinement ratio ( $\sigma_w/f_{co}$ ), peak stress ( $f_{cu}$ ), peak axial strain ( $\epsilon_{au}$ ), triaxial strength ratio ( $f_{au}/f_c$ ), and peak radial strain ( $\epsilon_{ru}$ ). The elastic modulus ( $E_{sec}$ ) is calculated based on the slope of the straight line from origin to the point of  $0.45f_c$  (Chen et al., 2019a). The peak stress and peak strain increase as the confining stress increases, which is mainly ascribed to two reasons. On the one hand, the elastic interval is enlarged as a sequence of the transverse constraint force provided by the confining pressure. On the other hand, the internal pores and attached old mortar inside the recycled aggregate are continuously squeezed, leading to increased plastic deformation. In terms of effect of recycling cycles, the peak stress decreases, whereas the peak strain presents an increasing-decreasing trend as the number of recycling cycles increases. The increasing number of recycling cycles will lead to the volume

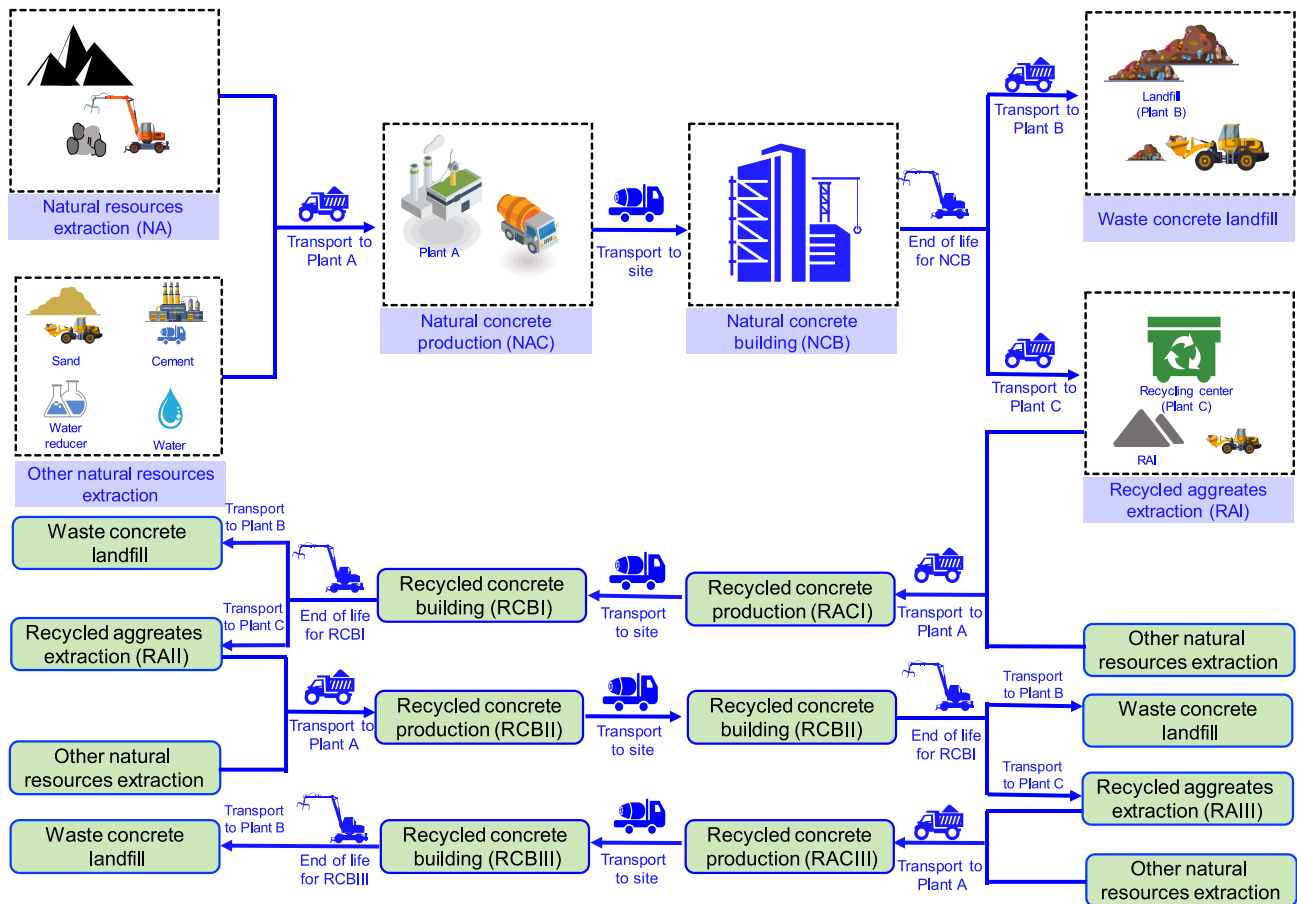


**Fig. 2.** The system boundary of NAC and three generations Multi-RAC based on ‘cradle-to-cradle’ LCA. Note: Plant A: Concrete mixing plant; Plant B: Waste concrete landfill; Plant C: Recycled aggregate recycling plant.

**Table 4**  
Life cycle inventory for concrete construction and demolition, waste concrete post-demolition treatment stages.

	Unit	Concrete construction (kg·m <sup>-3</sup> )	Concrete demolition (kg·m <sup>-3</sup> )	Waste concrete landfill (kg)	RA potential environmental benefits (kg)
GWP	kg CO <sub>2</sub> eq.	8.93E+00	8.03E+00	1.03E-03	-9.25E-04
ODP	kg CFC <sub>11</sub> eq.	8.81E-12	7.92E-12	-	-
POCP	kg C <sub>2</sub> H <sub>4</sub> eq.	1.28E+02	1.15E+02	2.53E-03	-2.27E-03
AP	kg SO <sub>2</sub> eq.	3.83E-02	3.44E-02	1.00E-05	-8.98E-06
EP	kg PO <sub>4</sub> eq.	9.54E-03	8.59E-03	-	-
CED	MJ	1.23E+02	1.11E+02	1.70E-02	-1.53E-02
Refs.	-	Gong et al. (Gong et al., 2012)	Gong et al. (Gong et al., 2012)	Ding et al. (Ding et al., 2016)	-

Note: According to Yang et al. (Yang et al., 2014) and Xiao et al. (Xiao et al., 2022b), the EI of 1 t of construction solid waste directly to landfill was - 0.898 times that of recycling to prepare recycled aggregates, the potential environmental benefits of RA were calculated. The distance from the demolition site to the landfill (Plant B) or the recycling centre (Plant C) is the same, 25 km, and the transportation is by truck (Xiao et al., 2022b).

reduction of natural coarse aggregate fraction and volume increment of attached old mortar (Thomas et al., 2018; Zhu et al., 2016), while the attached old mortar is able to increase the porosity and modify the deformation capacity of the concrete specimen. Moreover, the characteristics of the rough and multi-angular surface structure of Multi-RCA can enhance the friction force of Multi-RAC in the crack development process, thus increasing interlocking capacity and deformation resistance of the aggregate.

### 3.3. Multivariate regression analysis

The foregoing analysis evidenced that both the number of recycling cycles (n) and confining pressure (σ<sub>w</sub>) can influence the triaxial mechanical properties of the Multi-RAC. Multivariate regression analysis is performed to further investigate the inherent correlations between the influential factors (C<sub>n</sub> and σ<sub>w</sub>) and the triaxial mechanical properties (peak stress, peak strain, and elastic modulus). Referring to previous studies that predicted the strength behaviour of RAC (Jin et al., 2018a; Jin et al., 2018b), a series of potential regression models were established by linking the multiple independent variables (IVs) in different forms (linear, non-linear, and mixed methods). The conventional multivariate linear function relationship can be expressed as:

$$Y_i = \alpha + \beta_1 X_1 + \beta_2 X_2 + \dots + \beta_n X_n, i = 1, \dots, n, \text{linear model 1} \quad (1)$$

where α and β are regression constants. Y<sub>i</sub> denotes the response dependent variable (RDV) corresponding to the peak stress, peak strain, and elastic modulus in present study (n = 3). X<sub>i</sub> denotes the IVs corresponding to the confining pressure and the number of recycling cycles. The values of IVs are 0, 5, 10, 15, and 20 (confining pressure) and 0, 1, 2, and 3 (number of recycling cycles). In addition, by means of performing

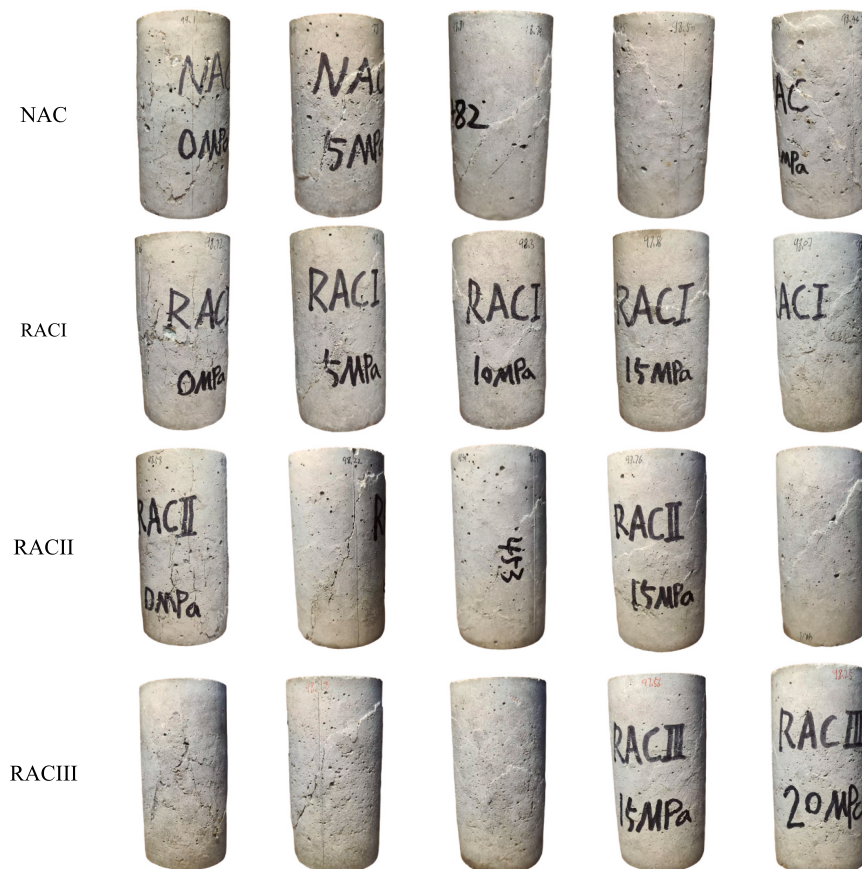


Fig. 3. Representative failure modes of four groups of concrete.

**Table 5**  
Triaxial mechanical results of four groups of specimens.

Group	$f_{co}$ (MPa), Cov (%)	$\sigma_w$ (MPa)	$\sigma_w/f_{co}$	$f_{cu}$ (MPa), Cov (%)	$f_{su}/f_{co}$	E (GPa)	$\epsilon_{cu}$ ( $\times 10^3$ )	$\epsilon_{ru}$ ( $\times 10^3$ )
NAC	43.7 (2.26)	0	0	43.7 (2.26)	1.00	16.0 (1.79)	3.9 (2.16)	1.94
		5	0.11	70.9 (3.55)	1.62	17.3 (4.04)	9.2 (6.16)	4.47
		10	0.23	95.7 (1.31)	2.19	15.7 (5.07)	11.6 (5.56)	3.03
		15	0.34	111.9 (4.57)	2.56	16.4 (4.61)	14.4 (2.55)	3.80
		20	0.46	118.6 (4.68)	2.71	15.6 (5.15)	19.4 (5.22)	4.53
RACI	30.5 (2.56)	0	0.00	30.5 (2.56)	1.00	9.6 (2.76)	5.27 (2.57)	3.98
		5	0.16	66.2 (3.37)	2.17	12.8 (2.21)	10.0 (6.19)	3.64
		10	0.33	83.8 (3.97)	2.75	13.2 (2.02)	16.4 (2.56)	6.07
		15	0.49	103.0 (4.41)	3.38	12.9 (2.97)	19.8 (6.37)	7.94
		20	0.66	116.1 (4.64)	3.81	11.7 (4.69)	26.9 (0.61)	7.90
RACII	34.5 (2.18)	0	0.00	34.5 (2.18)	1.00	10.0 (3.22)	5.0 (1.90)	3.06
		5	0.14	74.9 (3.69)	2.17	11.6 (3.22)	12.0 (2.52)	3.57
		10	0.29	92.8 (4.20)	2.69	14.4 (2.59)	15.1 (2.14)	3.56
		15	0.43	106.6 (2.29)	3.09	13.6 (4.02)	19.7 (6.33)	5.28
		20	0.58	113.7 (4.60)	3.30	11.8 (2.84)	25.6 (3.78)	5.43
RACIII	35.7 (2.13)	0	0.00	35.7 (2.13)	1.00	12.8 (2.46)	4.9 (2.31)	7.57
		5	0.14	68.2 (3.45)	1.91	17.1 (4.12)	8.2 (3.10)	3.77
		10	0.28	91.7 (4.17)	2.57	15.2 (5.45)	12.6 (6.25)	4.49
		15	0.42	102.3 (4.40)	2.87	16.2 (4.73)	15.9 (2.57)	6.81
		20	0.56	112.8 (1.55)	3.16	16.1 (1.32)	20.5 (1.98)	8.77

natural logarithm of the abovementioned conventional linear function or incorporating more mixed IVs, the following nonlinear and mixed model relationships expressed in multivariate linear formats were proposed to enable improved accuracy of the regression results.

$$\ln(Y_i) = \alpha + \beta_1 X_1 + \beta_2 X_2 + \dots + \beta_i X_i, i = 1, \dots, n, \text{nonlinear model 2} \quad (2)$$

$$\ln(Y_i) = \alpha + \beta_1 \ln(X_1) + \beta_2 \ln(X_2) + \dots + \beta_i \ln(X_i), i = 1, \dots, n, \text{nonlinear model 3} \quad (3)$$

$$\frac{X_{ik}}{Y_i} = \alpha + \sum_{j=1}^k \beta_j X_{ij}, i = 1, \dots, n, j = 1, \dots, k, \text{mixed models from 4 to } (k+3) \quad (4)$$

$$\frac{\ln(X_{ik})}{Y_i} = \alpha + \sum_{j=1}^k \beta_j \ln(X_{ij}), i = 1, \dots, n, j = 1, \dots, k, \text{mixed models from } (k+4) \text{ to } (2k+3) \quad (5)$$

A total of 7 multivariate regression models were presented for individual RDV as listed in Eqs. (1), (2), (3), (4), (5). Multivariate regression analysis on 60 sample data is performed with the assistance of SPSS software to ensure the desired accuracy. Variance and residual analysis were carried out for individual models. Meanwhile, the significance of individual influential factors was tested. The regression results of RDVs of peak stress, peak strain, and elastic modulus relative to the IVs of the number of recycling cycles and confining pressure are detailed in Table 6. The Durbin-Watson statistical results (D-W values) can be used

to autocorrelation of model residual deviations. The optimized range of D-W values is 1.5–2.5 and is preferably close to 2.0 (Xu et al., 2021).

As shown in Table 6, the mixed models outperform the linear models, especially for the RDV of elastic modulus. The E-related linear model and nonlinear models failed to fit the experimental data. After comprehensive considering both R<sup>2</sup> and D-W values, the best-fit multivariate regression models in predicting peak stress, peak strain, and elastic modulus were analyzed as the mixed models 5, 7 and 7, respectively. Their expressions are shown as follows:

$$\text{model 5: } \frac{X_{\sigma w}}{f_{cu}} = 0.014 + 0.001 * N + 0.008 * X_{\sigma w} \quad (R^2 = 0.956, D - W \text{ value} = 1.613) \quad (6)$$

$$\text{model 7: } \frac{\ln(X_{\sigma w})}{\epsilon_v} = -0.254 + 0.007 * \ln(X_{cn}) + 0.171 * \ln(X_{\sigma w}), \quad (R^2 = 0.964, D - W \text{ value} = 1.664) \quad (7)$$

$$\text{model 7: } \frac{\ln(X_{cn})}{E} = -0.033 - 0.003 * \ln(X_{cn}) + 0.082 * \ln(X_{\sigma w}) \quad (R^2 = 0.966, D - W \text{ value} = 1.950) \quad (8)$$

The histogram and cumulative probability of standardized residuals of the foregoing best-fit regression models are shown in Fig. 4. It is shown that the standardized residuals of peak stress, peak strain, and elastic modulus-related RDVs are generally consistent with the normal distribution, which are symmetrically distributed along the zero residual-axis. Figs. 4 (d), (e), and (f) compare the cumulative probability

**Table 6**  
Regression results of mechanical properties of NAC and Multi-RAC.

Regression models (Model No.)	$f_{cu}$ -related			$\epsilon_{cu}$ -related			E-related			
	RDV	R <sup>2</sup>	D-W value	RDV	R <sup>2</sup>	D-W value	RDV	R <sup>2</sup>	D-W value	
Linear model	1	$f_{cu}$	0.913	1.325	$\epsilon_{cu}$	0.827	0.773	E	0.054	0.810
Non-linear model	2	$\ln(f_{cu})$	0.822	1.584	$\ln(\epsilon_{cu})$	0.858	1.088	$\ln(E)$	0.066	0.872
	3	$\ln(f_{cu})$	0.893	1.591	$\ln(\epsilon_{cu})$	0.777	1.314	$\ln(E)$	0.382	0.779
Mixed model	4	$X_{cn}/f_{cu}$	0.761	1.520	$X_{cn}/\epsilon_{cu}$	0.767	1.469	$X_{cn}/E$	0.926	1.033
	5	$X_{\sigma w}/f_{cu}$	0.956	1.613	$X_{\sigma w}/\epsilon_{cu}$	0.726	1.161	$X_{\sigma w}/E$	0.945	1.092
	6	$\ln(X_{cn})/f_{cu}$	0.843	1.167	$\ln(X_{cn})/\epsilon_{cu}$	0.719	1.362	$\ln(X_{cn})/E$	0.995	1.433
	7	$\ln(X_{\sigma w})/f_{cu}$	0.972	1.577	$\ln(X_{\sigma w})/\epsilon_{cu}$	0.964	1.664	$\ln(X_{\sigma w})/E$	0.966	1.950

Note: R<sup>2</sup> refers to the goodness of fit; D-W value refers to Durbin-Watson statistical result;  $X_{cn}$  and  $X_{\sigma w}$ , are the abbreviations of IVs of the number of recycling cycles and confining pressure. Since value of 0 cannot be preceded with the natural logarithm, all 0 values in sample data are replaced by 0.001 to perform the regression analysis.

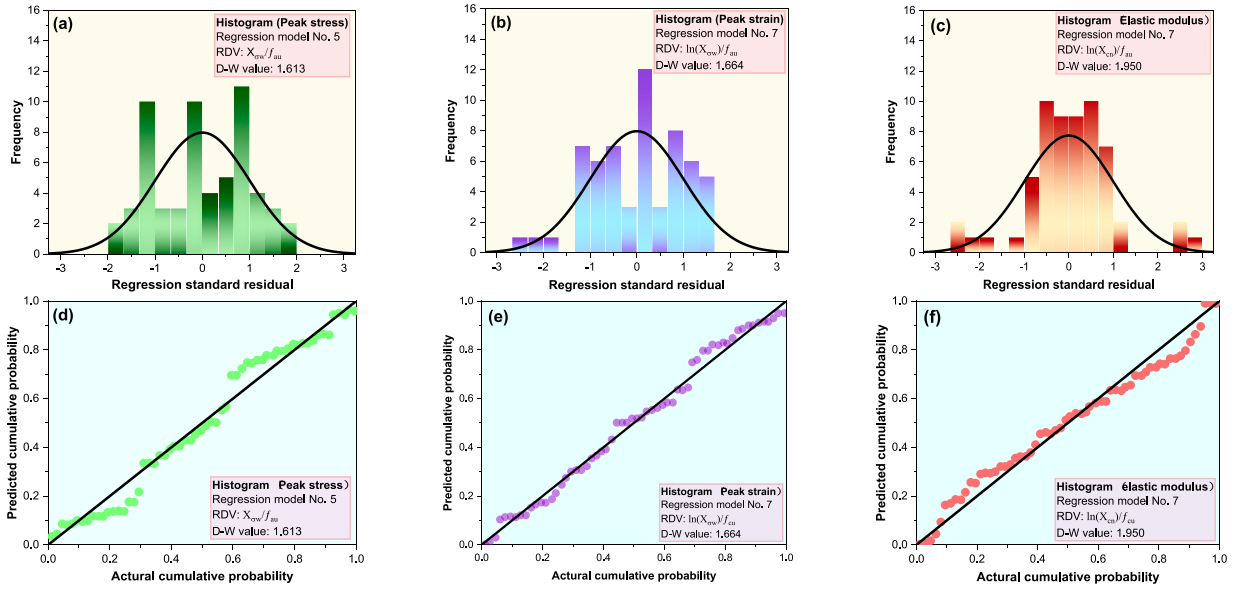


Fig. 4. Standardized residual histogram and normal probability using best-fit models.

distribution between the theoretical normal hypothesis and sample observations. It is evident that all residuals of RDVs-related models were evenly distributed on the two-sides of the 45-degree diagonal of the graph, further evidencing the reliability of the normal distribution hypothesis of sample residuals.

In addition, analysis of variance (ANOVA) and Spearman correlation analysis are employed to inherent effects of the number of regeneration cycles ( $C_n$ ) and confining pressure ( $\sigma_w$ ) on the triaxial mechanical properties of peak stress, peak strain, and elastic modulus. The results are illustrated in Table 7. All P-values for the number of recycling cycles and confining pressure with respect to peak stress, peak strain and elastic modulus are less than 0.05, while the P value for the confining pressure is less than 0.001. It is indicated that both the number of recycling cycles and confining pressure possess a significant effect on peak stress, peak strain, and elastic modulus, which show a close agreement with the results of mechanical behaviours as previously discussed. The results of Spearman correlation analysis indicate that the peak strain is positively correlated, whereas peak stress and elastic modulus are negatively correlated to the confining pressure. The main reasons are as follows. On the one hand, the increase of lateral confining pressure increases the elastic interval of the specimens, which makes the peak strain increase. On the other hand, the presence of high lateral confining pressure caused the microcracks on the RA surface to sprout and expand, resulting in a decrease in the peak stress and elastic modulus of the specimens. Additionally, the F values of peak stress and peak strain are relatively larger than that of the elastic modulus. Both the tested results agree that the number of recycling cycles and confining pressure possess the most significant effect on peak stress and the insignificant effect on elastic modulus.

#### 4. Conventional failure criteria

In this section, three conventional failure criteria, including Mohr-

Coulomb failure criterion, Power-Law failure criterion, and Willam-Warnke failure criterion were calibrated to acquire the failure criteria applicable to the Multi-RAC.

##### 4.1. Mohr-Coulomb failure criterion

With the advantages of simple form and certain accuracy, the Mohr-Coulomb failure criterion is one of the commonly used methods to study the failure envelope of brittle materials, often used to describe the strength of concrete materials under constrained loads (Xu et al., 2021). The compression meridian of the Mohr-Coulomb failure criterion is a straight line, thus the triaxial strength ratio ( $f_{cu}/f_{co}$ ) is linearly correlated to the confinement ratio ( $\sigma_w/f_{co}$ ).

$$\frac{f_{cu}}{f_{co}} = 1 + k \left( \frac{\sigma_w}{f_{co}} \right) \quad (9)$$

where  $k = (1 + \sin\varphi)/(1 - \sin\varphi)$  is the coefficient;  $\varphi$  denotes the internal friction angle. Based on the experimental data, the Mohr-Coulomb failure criterion equations for four groups of specimens are acquired as below.

$$\text{NAC} : \frac{f_{cu}}{f_{co}} = 1 + 4.230 \left( \frac{\sigma_w}{f_{co}} \right) \quad (R^2 = 0.992) \quad (10)$$

$$\text{RACI} : \frac{f_{cu}}{f_{co}} = 1 + 4.672 \left( \frac{\sigma_w}{f_{co}} \right) \quad (R^2 = 0.990) \quad (11)$$

$$\text{RACII} : \frac{f_{cu}}{f_{co}} = 1 + 4.619 \left( \frac{\sigma_w}{f_{co}} \right) \quad (R^2 = 0.979) \quad (12)$$

$$\text{RACIII} : \frac{f_{cu}}{f_{co}} = 1 + 4.357 \left( \frac{\sigma_w}{f_{co}} \right) \quad (R^2 = 0.988) \quad (13)$$

Table 7  
Results of ANOVA and Spearman correlation analysis.

RDVs (parameters)	Peak stress ( $f_{cu}$ )			Peak strain ( $\epsilon_{cu}$ )			Elastic modulus (E)		
	Correlation coefficient ( $\rho$ )	F value	P value	Correlation coefficient $\rho$	F value	P value	Correlation coefficient $\rho$	F value	P value
ANOVA	–	147.1	–	–	159.6	–	–	38.2	–
$C_n$	–0.054	10.8	0.000	0.008	97.8	0.000	–0.092	162.4	0.000
$\sigma_w$	0.956	685.9	0.000	0.912	638.3	0.000	0.219	36.6	0.000

As illustrated in Eqs. (10) to (13), the values of  $k$  for NAC, RACI, RACII, RACIII are 4.230, 4.672, 4.619, and 4.357, which corresponds to the internal friction angles of  $38.140^\circ$ ,  $40.345^\circ$ ,  $40.096^\circ$ , and  $38.804^\circ$ , respectively. With the increasing number of recycling cycles, the internal angle presents a first increase then decrease trend. It is indicated that the recycling cycles pose a downward trend of the internal cohesive force of the concrete, which agrees well with the results by Tang et al. (Tang et al., 2019). It is seen that with respect to the uniaxial compressive strength  $f_{co}$ , the increasing ratio of the peak stress of Multi-RAC is higher than NAC when the lateral stress is fixed at the same level, wherein the RACI is the highest and followed by RACII and RACIII. The trend of RACI compared to NAC is consistent with the model calibration study for the triaxial strength criterion of RCA (Li et al., 2022), which partially validates the results obtained in the present study. The higher sensitivity to the lateral confinement for RACI followed by RACII and RACIII compared to NAC should be ascribed to the fact that the adverse

effects of micro-cracks of recycled aggregate is significantly weakened by the lateral confinement (Li et al., 2022; Wang et al., 2020), while the additional recycling cycles reduce the sensitivity of RAC to lateral confinement.

Figs. 5 (a) and (b) compare the Mohr-Coulomb failure criterion equations with the experimental results from previous literature. The absence of comparisons for RACII and RACIII is owing to the unavailability of the database. The results show that the great discrete degree and the Mohr-Coulomb failure criterion equations underestimate the experimental results from the literature, which are further substantiated by Figs. 5 (c) and (d), which illustrate the comparison between the predictions by Mohr-Coulomb failure criterion equations and the experimental results. Three statistical indicators, including the average absolute error (AAE), the mean square error (MSE), and the standard deviation (SD), which are defined by Eqs. (14)–(16), were implemented to estimate the overall performance of the Mohr-Coulomb failure model.

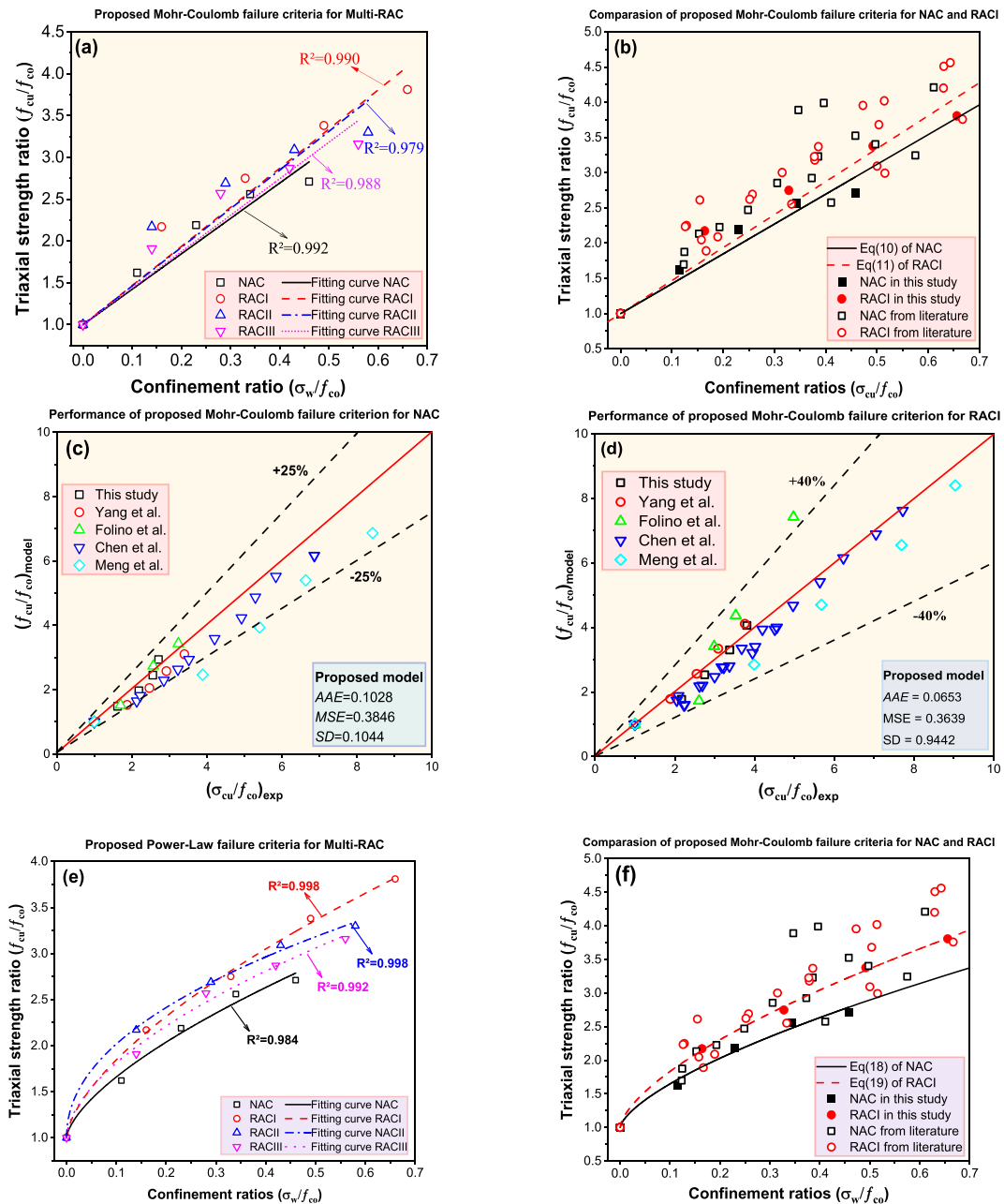


Fig. 5. Conventional failure criteria comparison and performance, data collected from (Folino and Xargay, 2014; Yang et al., 2011; Meng et al., 2020; Chen et al., 2015).

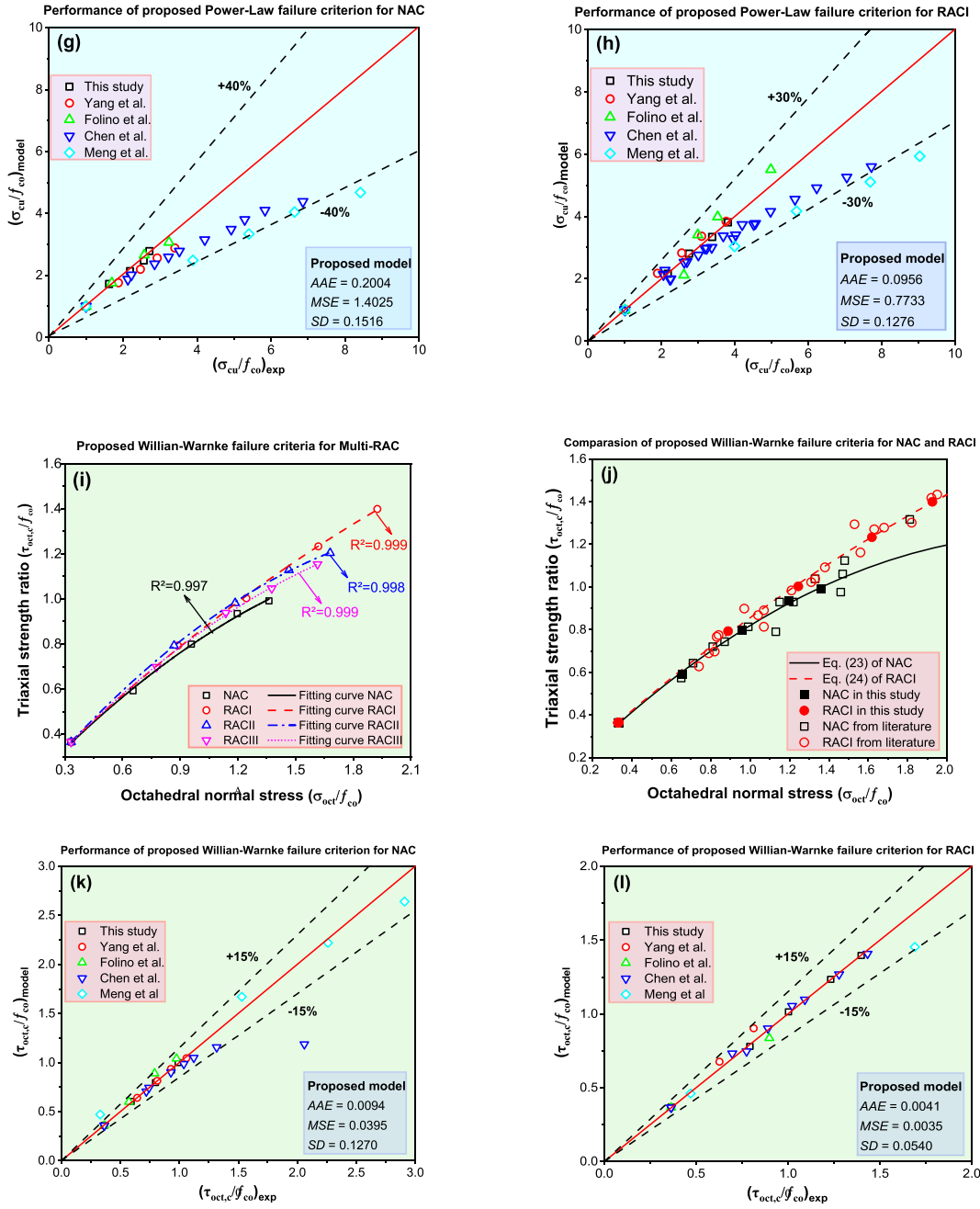


Fig. 5. (continued).

$$AAE = \frac{\sum_{i=1}^N \frac{mod_i - exp_i}{exp_i}}{N} \quad (14)$$

$$MSE = \frac{\sum_{i=1}^N (mod_i - exp_i)^2}{N} \quad (15)$$

$$SD = \sqrt{\frac{\sum_{i=1}^N \left[ \frac{mod_i}{exp_i} - \left( \frac{mod}{exp} \right)_{avg} \right]^2}{N-1}} \quad (16)$$

#### 4.2. Power-Law failure criterion

The foregoing analysis using Mohr-Coulomb failure criterion underestimates the influence of confining pressure on the axial peak strength of four groups of specimens, especially at a lower confinement

ratio, which is mainly ascribed to the fact that compression meridian derived from Mohr-Coulomb failure criterion is a straight line. Some scholars found a nonlinear expression might better describe the relationship between the axial peak stress and confining pressure of concrete materials (Yang et al., 2022; Khan et al., 2018). A nonlinear extension form of Mohr-Coulomb criterion, namely Power-Law failure criterion is given as:

$$\frac{f_{cu}}{f_{co}} = 1 + a \left( \frac{w}{f_{co}} \right)^b \quad (17)$$

where  $a$ ,  $b$  are the coefficients. Based on the experimental data, the Power-Law failure criterion equations for four groups of specimens are acquired as:

$$\text{NAC} : \frac{f_{cu}}{f_{co}} = 1 + 2.967 \left( \frac{\sigma_w}{f_{co}} \right)^{0.653} \quad (R^2 = 0.984) \quad (18)$$

$$\text{RACI} : \frac{f_{cu}}{f_{co}} = 1 + 3.677 \left( \frac{\sigma_w}{f_{co}} \right)^{0.638} \quad (R^2 = 0.998) \quad (19)$$

$$\text{RACII} : \frac{f_{cu}}{f_{co}} = 1 + 3.031 \left( \frac{\sigma_w}{f_{co}} \right)^{0.474} \quad (R^2 = 0.998) \quad (20)$$

$$\text{RACIII} : \frac{f_{cu}}{f_{co}} = 1 + 3.074 \left( \frac{\sigma_w}{f_{co}} \right)^{0.578} \quad (R^2 = 0.992) \quad (21)$$

Fig. 5 (e) and (f) illustrate the Power-Law failure criterion equations and their comparison with the experimental data from the literature. Fig. 5 (g) and (h) present the performance of predictions by equations and the experimental results. Similar to the Mohr-Coulomb failure criterion, the results also present a great discrete degree. The Power-law failure criterion equations also underestimate the experimental results from the literature, especially at higher confinement ratios. The predictive accuracy has not been improved by Power-Law failure criterion in comparison to Mohr-Coulomb failure criterion.

#### 4.3. Willam-Warnke failure criterion

The Willam-Warnke is a five-parameter model which is extensively implemented in predicting the failure behaviours of concrete and cohesive-frictional materials (Giraldo-Londoño and Paulino, 2020). In this model, the curved meridian is presented via the quadratic parabola expression, wherein the noncircular trace in the partial plane is approximated via the elliptic curve for individual part in the range of  $0 \leq \theta \leq 60^\circ$  (Yang et al., 2022). It can properly characterize the failure behaviour of concrete materials under both low and high hydrostatic stress by overcoming the deficiency of three parameters model. The stress condition in the present study is  $\sigma_1 > \sigma_2 = \sigma_3$  and the corresponding to Lode angle  $\theta$  of  $60^\circ$ . The compression meridian equation can be expressed as:

$$\frac{\tau_{oct,c}}{f_{co}} = a_0 + a_1 \left( \frac{\sigma_{oct}}{f_{co}} \right) + a_2 \left( \frac{\sigma_{oct}}{f_{co}} \right)^2 \quad (22)$$

where  $\sigma_{oct} = \frac{1}{3}(\sigma_1 + \sigma_2 + \sigma_3)$ ,  $\tau_{oct,c} = \frac{1}{15} \sqrt{(\sigma_1 - \sigma_2)^2 + (\sigma_2 - \sigma_3)^2 + (\sigma_1 - \sigma_3)^2}$ ;  $\sigma_{oct}$  and  $\tau_{oct,c}$  are the octahedral normal stress and octahedral shear stress of the compressive meridian, respectively. Based on the experimental data, the Willam-Warnke failure criterion equations for four groups of specimens are acquired as:

$$\text{NAC} : \frac{\tau_{oct,c}}{f_{co}} = 0.069 + 0.937 \left( \frac{\sigma_{oct}}{f_{co}} \right) - 0.186 \left( \frac{\sigma_{oct}}{f_{co}} \right)^2 \quad (R^2 = 0.998) \quad (23)$$

$$\text{RACI} : \frac{\tau_{oct,c}}{f_{co}} = 0.094 + 0.855 \left( \frac{\sigma_{oct}}{f_{co}} \right) - 0.093 \left( \frac{\sigma_{oct}}{f_{co}} \right)^2 \quad (R^2 = 0.999) \quad (24)$$

$$\text{RACII} : \frac{\tau_{oct,c}}{f_{co}} = 0.039 + 1.050 \left( \frac{\sigma_{oct}}{f_{co}} \right) - 0.211 \left( \frac{\sigma_{oct}}{f_{co}} \right)^2 \quad (R^2 = 0.999) \quad (25)$$

$$\text{RACIII} : \frac{\tau_{oct,c}}{f_{co}} = 0.061 + 0.969 \left( \frac{\sigma_{oct}}{f_{co}} \right) - 0.181 \left( \frac{\sigma_{oct}}{f_{co}} \right)^2 \quad (R^2 = 0.999) \quad (26)$$

Figs. 5 (i) and (j) illustrate the Willam-Warnke failure criterion equations and its comparison with the experimental data from the literature. Figs. 5 (k) and (l) present the performance of predictions by equations and the experimental results. It is shown that the Willam-Warnke failure criterion equations of both NAC and RACI present high coincidence with the experimental data from the reference. The slight underestimation of the NAC equation under a higher confinement ratio should be ascribed to the absence of test data in the present study.

Nevertheless, the errors of predictions by Willam-Warnke criterion equations are generally within  $\pm 15\%$ , demonstrating their good performance.

The foregoing analysis implies that Willam-Warnke failure criterion presents the highest predictive accuracy among the three conventional failure criteria for Multi-RAC. The correlation between its related parameters  $a_0$ ,  $a_1$  and  $a_2$ , and the number of recycling cycles  $c_n$  can be obtained via mathematic regression analysis:

$$a_0 = 0.0683 + 0.116c_n - 0.117c_n^2 + 0.0259c_n^3 \quad (R^2 = 0.998) \quad (27)$$

$$a_1 = 0.928 - 0.401c_n + 0.411c_n^2 - 0.0913c_n^3 \quad (R^2 = 0.981) \quad (28)$$

$$a_2 = -0.184 - 0.315c_n - 0.282c_n^2 + 0.0592c_n^3 \quad (R^2 = 0.997) \quad (29)$$

## 5. Modified elastoplastic model and non-integer high order failure criterion

### 5.1. Modelling

#### 5.1.1. General stress formulation

In general, the strain tensor is comprised by:

$$\varepsilon = \varepsilon^e + \varepsilon^p \quad (30)$$

where  $\varepsilon^e$  and  $\varepsilon^p$  are elastic and plastic components, respectively.

The stress formulation and its incremental formulation can be expressed as Eqs. (31) and (32):

$$\sigma = C_{eff} : \varepsilon^e = C_{eff} : (\varepsilon - \varepsilon^p) \quad (31)$$

$$d\sigma = C_{eff} : \varepsilon^e = C_{eff}(d\varepsilon - d\varepsilon^p) \quad (32)$$

where  $C_{eff}$  is the effective elastic stiffness tensor and can be given as:

$$C_{eff} = 2\mu k + 3kJ \quad (33)$$

where  $\mu$  and  $k$  are the shear and bulk modulus, respectively;  $k$  and  $J$  are four order tensors which define as the deviatoric and hydrostatic components, their components are given as  $J_{ijkl} = \frac{\delta_{ij}\delta_{kl}}{3}$  and  $K_{ijkl} = \frac{\delta_{ik}\delta_{jl} + \delta_{il}\delta_{jk}}{2} - J_{ijkl}$ .  $\delta$  is the second-order unit tensor. Moreover,  $\mu$  and  $k$  can be commonly expressed by the Young's modulus  $E$  and Poisson's ratio:

$$\mu = A = \frac{E}{2(1+\nu)} \quad (34)$$

$$k = A = \frac{E}{3(1-2\nu)} \quad (35)$$

As discussed previously, the elastic parameter  $E$  is related to the number of recycling cycles, while  $\nu$  is nearly unchanged with different number of recycling cycles.

#### 5.1.2. Non-integer high order failure criterion

To mitigate the defect that conventional models cannot properly predict the deformation characteristics, a non-integer high order failure criterion is proposed, which has improved adaptability than conventional linear and quadratic failure criteria (Xue et al., 2023):

$$F = \left( \frac{q}{P_r} \right)^n + A \left( \frac{p-C}{P_r} \right) = 0 \quad (36)$$

where,  $q$  and  $p$  are expressed as  $\sqrt{\frac{3}{2}(K:\sigma):(K:\sigma)}$  and  $\frac{1}{3}\text{tr}(\sigma)$ , respectively. The parameters  $n$  and  $A$  are shape control factor;  $C$  denotes the uniaxial tensile strength, which can be simplified as splitting tensile strength in many cases.  $P_r$  is a fixed parameter to assure the dimensionless form of the failure criterion.

### 5.1.3. Plastic yield function and plastic hardening law

Based on the failure criterion, the plastic yield function is proposed:

$$f = \left(\frac{q}{P_r}\right)^n + \alpha_p A \left(\frac{p-C}{P_r}\right) = 0 \quad (37)$$

where,  $\alpha_p$  denotes the plastic hardening. The plastic hardening process initiates and further intensifies as the plastic deformation proceeds. The plastic yield function coincides with the failure criterion once the material is damaged. The value of  $\alpha_p$  is in the range between 0 and 1.

With the consideration of monotone hardening characteristic, the plastic hardening can be given as:

$$\alpha_p = \alpha_p^0 + (1 - \alpha_p^0) \frac{\gamma_p}{B + \gamma_p} \quad (38)$$

where B denotes control parameter for hardening ratio and,  $\alpha_p^0$  is the initial plastic threshold which can be simplified as 0 in many cases.  $\gamma_p$  is the generalized plastic distortion and the increment form of  $\gamma_p$  can be expressed as:

$$d\gamma_p = \frac{\sqrt{\frac{2}{3}(K : \varepsilon^p)(K : \varepsilon^p)}}{B + \gamma_p} = \frac{h}{\chi_p}, h = \sqrt{\frac{2}{3}(K : \varepsilon^p)(K : \varepsilon^p)} \quad (39)$$

where  $\chi_p$  refers to regularizing parameter to consider the larger plastic strain under high confining pressure, which can be expressed as a function of minor principal stress:

$$\chi_p = \exp\left(\beta \frac{(-\sigma_3) \bullet |\sigma_3|}{P_r}\right) \quad (40)$$

where  $\beta$  is confining pressure dependent parameter and bracket  $\langle x \rangle$  denotes  $\langle x \rangle = (x + |x|)/2$ .

### 5.1.4. Plastic flow rule

The evolution of plastic strain can be described by the associated plastic flow. An associated plastic flow rule is proposed, and the plastic potential function can be expressed in the identical form as the yield criterion:

$$g = \left(\frac{q}{P_r}\right)^n + \chi_p A \left(\frac{p-C}{P_r}\right) \quad (41)$$

Once the plastic mechanism has been activated, the plastic strain increment can be expressed as:

$$d\varepsilon^p = d\lambda \frac{\partial g}{\partial \sigma} \quad (42)$$

where  $d\lambda$  denotes the plastic factor of the plastic mechanism.

Since the plastic yield criterion remains active when initial plastic yield surface is reached, the plasticity consistency condition can be expressed as:

$$df = \frac{\partial f}{\partial \sigma} \partial \sigma + \frac{\partial f}{\partial \gamma_p} \partial \gamma_p = 0 \quad (43)$$

By combing the Eqs. (32), (39), (42) and (43), the plastic factor can be expressed as:

$$d\lambda = \frac{\frac{\partial f}{\partial \sigma} : C : d\varepsilon}{\frac{\partial f}{\partial \sigma} : C : \frac{d\varepsilon}{\partial \sigma} - \frac{\partial f}{\partial \gamma_p} \frac{h}{\chi_p}} \quad (44)$$

Once  $d\lambda$  is decided, the plastic strain increment can be acquired through Eq. (44).

## 5.2. Simulated stress-strain curves

The abovementioned model is coded as a subroutine in the THMPASA program. The failure criterion curve of concrete materials

can be derived through the continuous iteration of stress, strain, and internal variables with increasing loading steps. The detailed iterative process can refer to authors' previous study (Xue et al., 2023). In terms of the parameter determination, there are seven essential parameters in the proposed mode including two elastic parameters ( $E$  and  $\nu$ ), three parameters ( $A$ ,  $C$ , and  $n$ ) determining the failure surface and two plastic parameters ( $B$  and  $\beta$ ). The elastic modulus  $E$  and  $\nu$  can be acquired from the initial linear elastic stage of the uniaxial stress-strain curve.  $A$  and  $n$  can be ascertained by the failure criterion equation and the best fitting effect between the  $p - q$  surface and failure surface. The parameters of  $B$  and  $\beta$  can be determined by the plastic hardening rule. Based on the experimental data and Eq. (38), the  $\alpha_p - \gamma_p$  curve at triaxial tests can be described in Fig. 6, the relevant parameters for the Multi-RAC with different number of recycling cycles are shown in Table 8. The comparison between experimental data and numerical simulations is shown in Figs. 7 (a) to (d), which shows a good agreement. The correlation between those  $C_n$  dependent parameters  $E$ ,  $n$ ,  $C$ ,  $A$  and  $C_n$  can be obtained via mathematical regression:

$$E = 15.800 - 11.2c_n - 5.54c_n^2 - 0.726c_n^3 \quad (R^2 = 0.998) \quad (45)$$

$$n = 1.215 - 0.0025c_n - 0.00025c_n^2 \quad (R^2 = 0.990) \quad (46)$$

$$C = 5.634 - 4.431c_n + 2.681c_n^2 - 0.467c_n^3 \quad (R^2 = 0.998) \quad (47)$$

$$A = 5.566 - 0.2570c_n + 0.0330c_n^2 \quad (R^2 = 0.999) \quad (48)$$

To further examine the validity of the proposed model, Figs. 7 (e) and (f) illustrate the non-integer high order failure criterion equations and their comparison with the experimental data from the literature. It is seen that although the proposed equations underestimate few experimental data reported by Folino et al. (Folino and Xargay, 2014), the errors of predictions by the proposed non-integer high order failure criterion equations are generally within  $\pm 10\%$ , demonstrating their good performance. The *AAE*, *MSE* and *SD* values of high order failure criterion compared to those of three conventional failure criteria are summarized in Table 9. Willam-Warke failure criterion presents the least statistic indicator values of 0.0094 (*AAE*, *NAC*), 0.0041 (*AAE*, *RACI*), 0.0035 (*MSE*, *RACI*) and 0.1270 (*SD*, *RACI*) while non-integer high order failure criterion presents the least statistic indicator values of 0.02353 (*MSE*, *NAC*) and 0.1207 (*SD*, *NAC*). Based on the statistic indicator values, the performance of four criteria is deemed in an order of: Non-integer high order  $\cong$  Willam-Warke  $>$  Mohr-Coulomb  $>$  Power-Law. In particular, the proposed non-integer high order failure

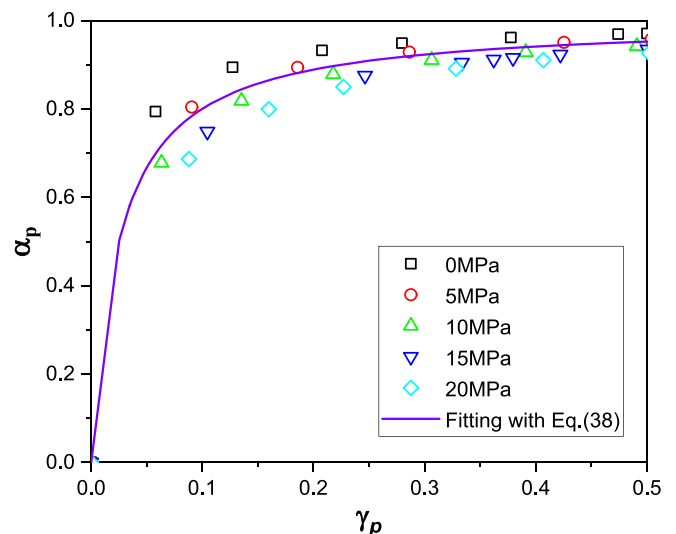


Fig. 6. Evolution of the hardening function for NAC.

**Table 8**  
Model parameters for NAC and three generations of Multi-RAC.

Group	$C_n$	E (GPa)	$\nu$	n	A	C (MPa)	B	$\beta$
NAC	0	16.0	0.18	1.215	5.565	5.691	2.5E-4	0.25
RAC <sub>1</sub>	1	9.6	0.18	1.213	5.343	3.452	2.5E-4	0.25
RAC <sub>2</sub>	2	10.0	0.18	1.211	5.182	3.799	2.5E-4	0.25
RAC <sub>3</sub>	3	12.8	0.18	1.210	5.092	3.902	2.5E-4	0.25

Note: C is related to the indirect tensile strength and is not tested. In general, C can be chosen in the range of  $1/15$  to  $1/8f_c$ .

criterion can properly predict and distinguish the deformation characteristics of both elastic and plastic stages in the pre-peak curve.

### 5.3. Life cycle analysis

#### 5.3.1. Environmental impact analysis

Table 10 and Fig. 8 (a) shows all EI indicators except for ODP decrease continuously with the increasing number of recycling cycles. In particular, CED and EP showed the most significant decline, reaching 50.66 % and 41.97 %, respectively. POCP showed the least significant decline, only 3.42 %. This is mainly due to the following two aspects. On the one hand, the transportation distance of RA from the waste concrete recycling center (Plant C) to the concrete preparation plant (Plant A) is much lower than that of NA from the natural resource extraction plant to the concrete preparation plant, as shown in Table 4. On the other hand, direct landfilling of waste concrete produces an adverse environmental effect, whereas recycling and preparing it into RA produces a potentially positive environmental effect. Meanwhile, the superposition of the two effects makes the environmental benefits of the Multi-RAC environmental benefits higher than those of NAC. Interestingly, the ODP value for three generations of Multi-RAC are 23.5 % ~ 23.7 % higher than that of NAC. This is mainly attributed to the fact that RA has a much higher ODP emission factor at the raw materials extraction stage than that of NA. Thus, special consideration should be considered how to mitigate the adverse impact of Multi-RAC contributing to ODP in raw material extraction stage.

#### 5.3.2. Analysis of proportions of GWP and CED

Fig. 8 (b) indicates that the raw materials extraction stage is the main source of concrete carbon emissions, which is consistent with Xiao et al. (Xiao et al., 2016). It mainly stems from the fact that cement production has the predominant contribution to the EI of concrete. Specifically, the carbon emissions caused by the cement production stage all account for more than 80 % of the entire life cycle of four generations of concrete. In addition, compared with NAC, the carbon emission contribution of three generations Multi-RAC in the raw materials transportation stage is reduced, mainly because the use of RA can reduce the carbon emission generated during the raw materials transportation. Moreover, previous research has shown that the EI of the transportation stage is the second most influential element in the life cycle of concrete after cement production (Xing et al., 2022). Therefore, recycling waste concrete into recycled aggregates makes the three generations of Multi-RAC more sustainable than conventional NAC.

Fig. 8 (c) provides that NAC and three generations of Multi-RAC have the most significant contribution to CED at the raw materials extraction, reaching more than 80 %. This is also related to cement production, which accounts for 69.9 % to 82.6 % of the energy consumption of the whole life cycle for four generations of concrete. In addition, as the increase of recycling cycles, the potential environmental compensation for three generations Multi-RAC become more significant. Specifically, RACIII has the best potential for environmental compensation, with carbon emissions and energy consumption accounting for 13.1 % and 43.5 %, respectively.

## 6. Conclusions

This study systematically investigated the mechanical properties and failure modes of NAC and three generations of Multi-RAC under the confined triaxial stress condition. Three conventional failure criteria and one newly proposed non-integer high order failure criterion were analyzed and calibrated. Finally, the life cycle assessment on Multi-RAC was conducted. The following can be drawn based on the experimental results and theoretical findings as below:

- (1) The triaxial failure modes of Multi-RAC are similar to conventional concrete, which presents the oblique shear cracks under triaxial compression. The triaxial failure mode is significantly affected by the confining pressure whereas it is insignificantly affected by the recycling cycles. Compared to NAC, the uniaxial compressive strength, the peak strain, and the elastic modulus of Multi-RAC are reduced by 18.3 % to 30.2 %, increased by 25.6 % to 35.1 % and reduced by 20 % to 40 %, respectively. With the improvement of confinement stress from 0 MPa to 20 MPa, the peak stress and peak strain are monotonically increased as the confinement stress increases, which are enlarged by 171.4 % to 280.6 % and 397.4 % to 412.0 %, respectively. Differently, elastic modulus presents an increasing-decreasing trend. In terms of the effect of recycling cycles, the peak stress decreases, whereas the peak strain presents an increasing-decreasing trend as the number of recycling cycles increases.
- (2) The proposed multivariate regression mixed models could properly estimate the triaxial mechanical properties of peak stress, peak strain, and elastic modulus within a given range of confinement pressures (0–20 MPa) and number of recycling cycles (0–3). All P-values for the number of recycling cycles and confining pressure with respect to peak stress, peak strain and elastic modulus are less than 0.05, while the P value for the confining pressure is less than 0.001 indicating both affect the mechanical properties of NAC and three generations of Multi-RAC, while the confining pressure possesses an even more significant effect. In particular, the Spearman correlation analysis indicate that the number of regeneration cycles and confining pressure possess the significant effect on the peak stress while presenting less effect on the elastic modulus.
- (3) Among three conventional failure criteria, the Willam-Warke failure criterion performs the best for Multi-RAC, which is substantiated by the least AAE values of 0.0094 and 0.0041, MSE values of 0.0395 and 0.0035, SD values of 0.1270 and 0.0540, respectively for NAC and RACI. Additionally, the relevant failure criterion is proposed for Multi-RAC with proper consideration of the effects of the lateral confining ratio and the number of recycling cycles.
- (4) With the proper iterative and calibration process, an elastoplastic model consisting of failure criterion, plastic criterion, and associated flow rule was proposed with the introduction of the number of recycling cycles into the model's parameters. The proposed model can properly simulate the triaxial stress-strain curves with acceptable deviation. Moreover, it seems that the dependence of plastic deformation be gradually decreased with increasing confining pressure.
- (5) The non-integral high order failure criterion derived modified elastic model presents the least statistic indicator values of 0.02353 (MSE, NAC) and 0.1207 (SD, NAC), showing a comparable good performance compared to the Willam-Warke failure criterion and outcomes the other two conventional criteria. The relative comparison with available data from the literature indicates although the proposed failure criterion underestimates a few experimental data reported by Folino et al. (Folino and Xargay, 2014), the errors of predictions by the proposed non-

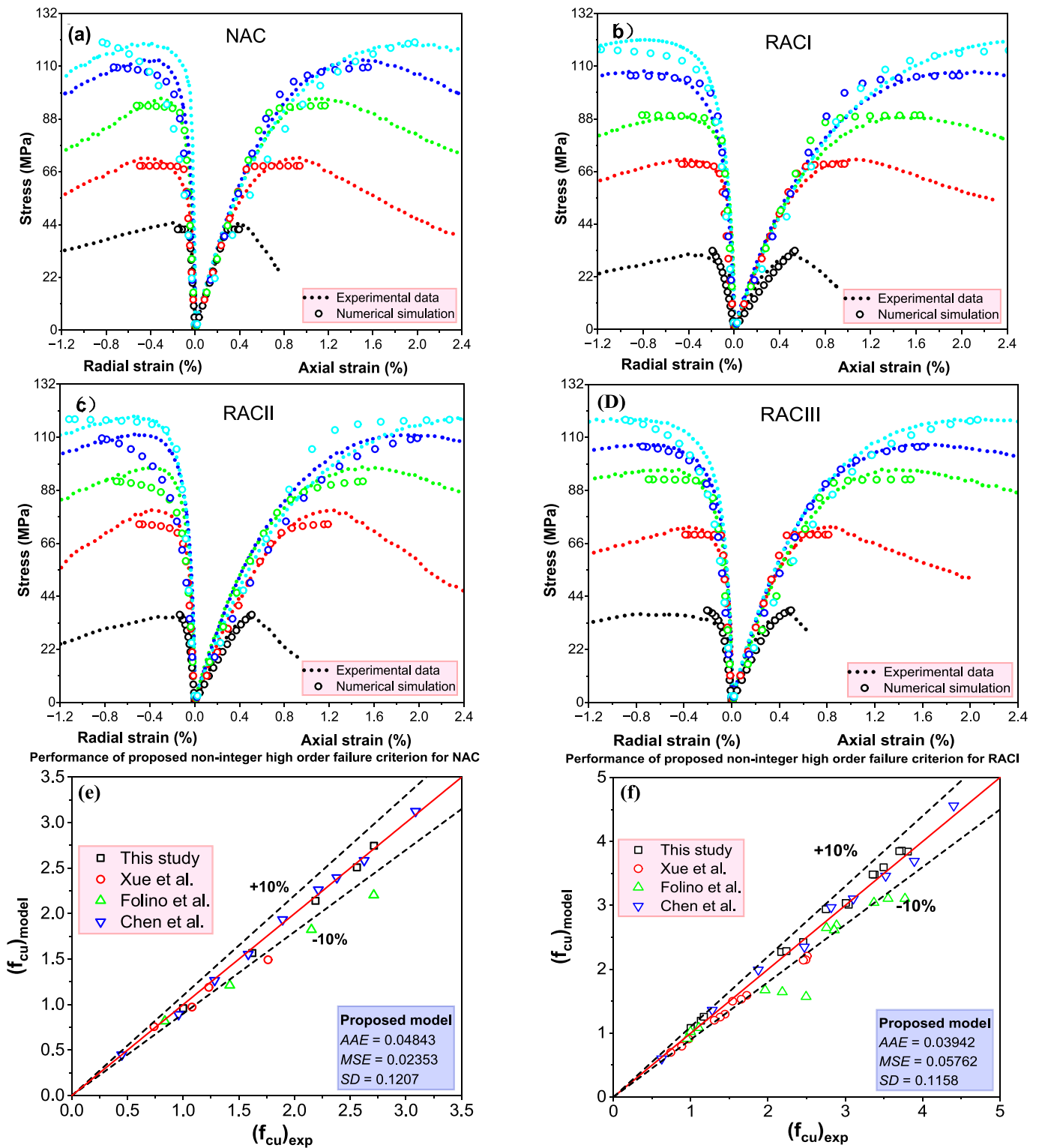


Fig. 7. Comparison between experimental data and numerical simulation and performance of the proposed model, data collected from (Folino and Xargay, 2014; Yang et al., 2011; Chen et al., 2015).

integer high order failure criterion equations are generally within  $\pm 10\%$ .

- (6) All EI indicators except for ODP decrease continuously with the increasing number of recycling cycles wherein CED and EP showed the most significant decline. Compared with NAC, GWP, POCP, AP, EP, and CED pertaining to RACIII are descended by 15.8 %, 3.24 %, 38.6 % 50.6 %, and 41.1 %, respectively. As the

number of recycling cycles increases, the potential environmental compensation for three generations of Multi-RAC becomes more significant. With carbon emissions and energy consumption accounting for 13.1 % and 43.5 % of the energy consumption of the whole life cycle, respectively.

- (7) It is worth pointing out that the proposed model and derived failure criterion have been primarily verified by comparing the

**Table 9**

AAE, MSE and SD values of three conventional failure criteria and non-integer high-order failure criterion.

Statistic indicator	Mohr-Coulomb		Power-Law		Willam-Warnke		Non-integer high order	
	NAC	RACI	NAC	RACI	NAC	RACI	NAC	RACI
AAE	0.1028	0.0653	0.2004	0.0956	0.0094	0.0041	0.04843	0.03942
MSE	0.3846	0.3639	1.4025	0.7733	0.0395	0.0035	0.02353	0.05762
SD	0.1044	0.9442	0.1516	0.1276	0.1270	0.0540	0.1207	0.1158

**Table 10**

EI results for NAC and three generations of Multi-RAC.

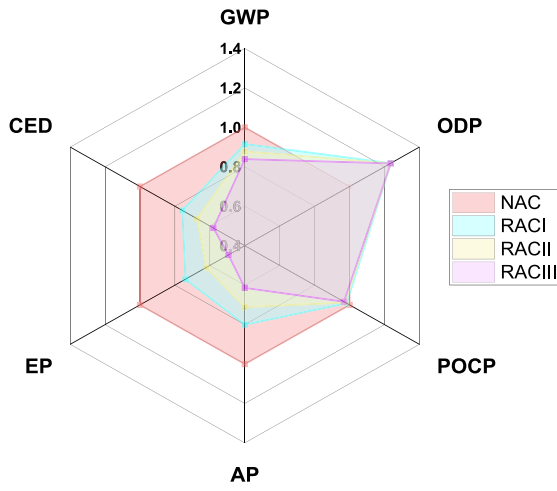
	NAC	RACI	RACII	RACIII
GWP/ kg CO <sub>2</sub> eq.	502.1	459.6	441.2	422.8
ODP/ kg CFC <sub>11</sub> eq.	3.72E-07	4.61E-07	4.60E-07	4.60E-07
POCP/ kg C <sub>2</sub> H <sub>4</sub> eq.	308.8	303.7	301.2	298.8
AP/ kg SO <sub>2</sub> eq.	0.9079	0.7265	0.6458	0.5570
EP/ kg PO <sub>4</sub> eq.	0.1523	0.1126	0.0946	0.0752
CED/ MJ	3042.4	2304.6	2048.3	1791.9

NAC and RACI data from previous literature. Future efforts can be placed on further validation of the proposed model, especially the applicability of empirical functions for the effects of recycling cycles (i.e., Eqs. (45)–(48)), once more data for RACII and RACIII

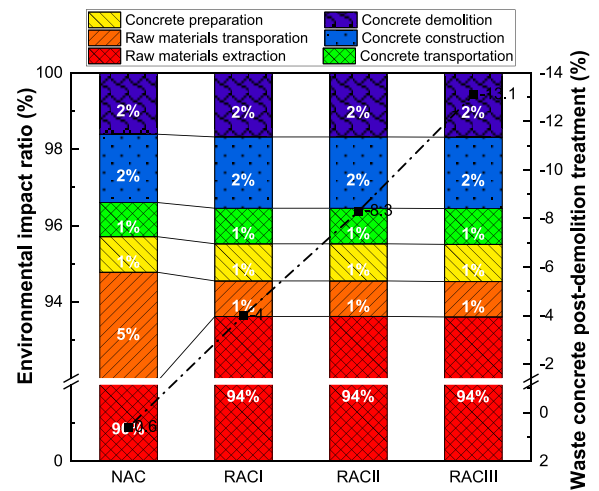
are available. In addition, the effects of an extensive range of confining pressure and other environmental factors, such as high-temperature exposure (Xu et al., 2021; Meng et al., 2017), curing effect (Chen et al., 2019b), and sulphate attack (Wei et al., 2019) etc., on the triaxial behaviours of Multi-RAC are worthily explored, to enable further advancement in establishing a more generalized model and understanding the long-term performance of the Multi-RAC under various environments and load conditions.

**CRedit authorship contribution statement**

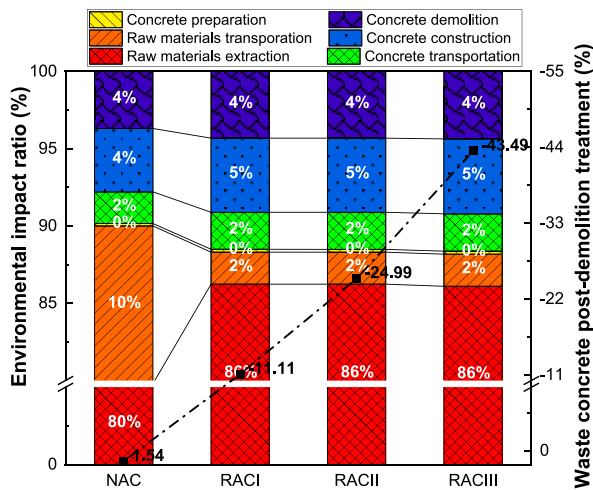
**Bin Lei:** Writing – review & editing, Writing – original draft, Validation, Supervision, Resources, Investigation, Funding acquisition,



(a) EI indicators (Normalized value)



(b) GWP



(c) CED

**Fig. 8.** EI analysis of NAC and three generations of Multi-RAC.

Formal analysis, Conceptualization. **Linjie Yu:** Writing – review & editing, Writing – original draft, Methodology, Investigation, Funding acquisition, Formal analysis, Data curation. **Yipu Guo:** Writing – review & editing, Writing – original draft, Validation, Investigation. **Hongjie Xue:** Writing – review & editing, Writing – original draft, Methodology, Investigation. **Xiaonan Wang:** Writing – review & editing, Writing – original draft, Validation. **Yan Zhang:** Writing – review & editing, Writing – original draft. **Wenkui Dong:** Writing – review & editing, Writing – original draft. **Frank Dehn:** Writing – review & editing, Writing – original draft. **Wengui Li:** Writing – review & editing, Writing – original draft, Validation, Supervision, Resources, Conceptualization.

### Declaration of competing interest

The authors declare that they have no known competing financial interests or personal relationships that could have appeared to influence the work reported in this paper.

### Data availability

Data will be made available on request.

### Acknowledgement

The authors would like to acknowledge the supports from National Natural Science Foundation of China (52268043, 51968046), Training Plan for Academic and Technical Leaders of Major Disciplines in Jiangxi Province-Leading Talent Project (20204BCJ22003), and the Australian Research Council (ARC), Australia. The third and fifth authors (Yipu Guo and Xiaonan Wang) also appreciate the China Scholarship Council (CSC). The last author (Wengui Li) also thanks the International Excellence Fellowship of Karlsruhe Institute of Technology (KIT), Germany.

### Appendix A. Supplementary data

Supplementary data to this article can be found online at <https://doi.org/10.1016/j.scitotenv.2024.171381>.

### References

- Akçaoğlu, T., 2017. Determining aggregate size & shape effect on concrete microcracking under compression by means of a degree of reversibility method. *Constr. Build. Mater.* 143, 376–386.
- Bahraq, A.A., Jose, J., Shameem, M., Maslehuddin, M., 2022. A review on treatment techniques to improve the durability of recycled aggregate concrete: enhancement mechanisms, performance and cost analysis. *Journal of Building Engineering* 55, 104713.
- Borges, P.M., Schiavon, J.Z., da Silva, S.R., Rigo, E., Junior, A.N., Possan, E., de Oliveira Andrade, J.J., 2023. Mortars with recycled aggregate of construction and demolition waste: mechanical properties and carbon uptake. *Constr. Build. Mater.* 387, 131600.
- Braga, A.M., Silvestre, J.D., de Brito, J., 2017. Compared environmental and economic impact from cradle to gate of concrete with natural and recycled coarse aggregates. *J. Clean. Prod.* 162, 529–543.
- Chen, Z., Chen, Y., Xu, J., Xue, J., 2015. Experimental study on failure criterion and stress-strain constitutive equation of recycled coarse aggregate concretes under triaxial compression. *China Civil Eng. J* 48 (12), 23–33.
- Chen, Y., Chen, Z., Xu, J., Lui, E.M., Wu, B., 2019a. Performance evaluation of recycled aggregate concrete under multiaxial compression. *Constr. Build. Mater.* 229, 116935.
- Chen, D., Yu, X., Liu, R., Li, S., Zhang, Y., 2019b. Triaxial mechanical behavior of early age concrete: experimental and modelling research. *Cem. Concr. Res.* 115, 433–444.
- Chen, Y., Li, P., Ye, P., Li, H., Liang, X., 2022. Experimental investigation on the mechanical behavior of polyvinyl alcohol fiber recycled aggregate concrete under triaxial compression. *Constr. Build. Mater.* 350, 128825.
- Chen, Y., He, Q., Liang, X., Chen, Z., Li, H., 2023. Experimental investigation on mechanical properties of steel fiber reinforced recycled aggregate concrete under uniaxial cyclic compression. *Constr. Build. Mater.* 387, 131616.
- Chiaia, B., Van Mier, J., Vervuurt, A., 1998. Crack growth mechanisms in four different concretes: microscopic observations and fractal analysis. *Cem. Concr. Res.* 28 (1), 103–114.
- De Juan, M.S., Gutiérrez, P.A., 2009. Study on the influence of attached mortar content on the properties of recycled concrete aggregate. *Constr. Build. Mater.* 23 (2), 872–877.
- Dey, D., Srinivas, D., Panda, B., Suraneni, P., Sitharam, T., 2022. Use of industrial waste materials for 3D printing of sustainable concrete: a review. *J. Clean. Prod.* 340, 130749.
- Ding, T., Xiao, J., Tam, V.W., 2016. A closed-loop life cycle assessment of recycled aggregate concrete utilization in China. *Waste Manag.* 56, 367–375.
- Dong, W., Li, W., Shen, L., Sheng, D., 2019. Piezoresistive behaviours of carbon black cement-based sensors with layer-distributed conductive rubber fibres. *Mater. Des.* 182, 108012.
- Folino, P., Xargay, H., 2014. Recycled aggregate concrete–mechanical behavior under uniaxial and triaxial compression. *Constr. Build. Mater.* 56, 21–31.
- Giraldo-Londoño, O., Paulino, G.H., 2020. A unified approach for topology optimization with local stress constraints considering various failure criteria: von Mises, Drucker–Prager, Tresca, Mohr–Coulomb, Bresler–Pister and Willam–Warnke. *Proceedings of the Royal Society A* 476 (2238), 20190861.
- Gonçalves, T., Silva, R., De Brito, J., Fernández, J., Esquinas, A., 2020. Mechanical and durability performance of mortars with fine recycled concrete aggregates and reactive magnesium oxide as partial cement replacement. *Cem. Concr. Compos.* 105, 103420.
- Gong, X., Nie, Z., Wang, Z., Cui, S., Gao, F., Zuo, T., 2012. Life cycle energy consumption and carbon dioxide emission of residential building designs in Beijing. *J. Ind. Ecol.* 16 (4), 576–587.
- Huang, Q., Qian, Z., Hu, J., Zheng, D., Chen, L., Zhang, M., Yu, J., 2021. Investigation on the properties of aggregate-mastic interfacial transition zones (ITZs) in asphalt mixture containing recycled concrete aggregate. *Constr. Build. Mater.* 269, 121257.
- Huda, S.B., Alam, M.S., 2014. Mechanical behavior of three generations of 100% recycled recycled coarse aggregate concrete. *Constr. Build. Mater.* 65, 574–582.
- Jin, R., Chen, Q., Soboyejo, A.B., 2018a. Non-linear and mixed regression models in predicting sustainable concrete strength. *Constr. Build. Mater.* 170, 142–152.
- Jin, R., Yan, L., Soboyejo, A.B., Huang, L., Kasal, B., 2018b. Multivariate regression models in estimating the behavior of FRP tube encased recycled aggregate concrete. *Constr. Build. Mater.* 191, 216–227.
- Ke, G., Duanxiong, K., Zhang, X., Tang, Z., Yang, R., Li, W., 2023. Synthesis of quaternary hydroxylated carbon nanotube composite and its sulfate adsorption performance in cement paste. *J. Mater. Civ. Eng.* 35 (11), 04023400.
- Khan, M.Z.N., Hao, Y., Hao, H., Shaikh, F.U.A., Liu, K., 2018. Mechanical properties of ambient cured high-strength plain and hybrid fiber reinforced geopolymer composites from triaxial compressive tests. *Constr. Build. Mater.* 185, 338–353.
- Kim, J., Yang, S., Kim, N., 2023. Effect of plasticizer dosage on properties of multiple recycled aggregate concrete. *J. Mater. Cycles Waste Manage.* 25 (3), 1457–1469.
- Kisku, N., Joshi, H., Ansari, M., Panda, S., Nayak, S., Dutta, S.C., 2017. A critical review and assessment for usage of recycled aggregate as sustainable construction material. *Constr. Build. Mater.* 131, 721–740.
- Knoeri, C., Sanyé-Mengual, E., Althaus, H.-J., 2013. Comparative LCA of recycled and conventional concrete for structural applications. *Int. J. Life Cycle Assess.* 18, 909–918.
- Lei, B., Li, W., Tang, Z., Tam, V.W., Sun, Z., 2018. Durability of recycled aggregate concrete under coupling mechanical loading and freeze-thaw cycle in salt-solution. *Constr. Build. Mater.* 163, 840–849.
- Lei, B., Li, W., Tang, Z., Li, Z., Tam, V.W., 2020. Effects of environmental actions, recycled aggregate quality and modification treatments on durability performance of recycled concrete. *J. Mater. Res. Technol.* 9 (6), 13375–13389.
- Lei, B., Yu, H., Guo, Y., Dong, W., Liang, R., Wang, X., Lin, X., Wang, K., Li, W., 2023a. Fracture behaviours of sustainable multi-recycled aggregate concrete under combined compression-shear loading. *Journal of Building Engineering* 72, 106382.
- Lei, B., Yu, H., Guo, Y., Zhao, H., Wang, K., Li, W., 2023b. Mechanical properties of multi-recycled aggregate concrete under combined compression-shear loading. *Eng. Fail. Anal.* 143, 106910.
- Lei, B., Yu, L., Chen, T., Lv, Z., Zaland, S., Tang, Z., 2023c. Experimental study on the initial damage and mechanical property evolution of recycled coarse aggregates under freeze-thaw cycles and repeated loads. *Constr. Build. Mater.* 375, 130972.
- Li, L., Xiao, J., Xuan, D., Poon, C.S., 2018. Effect of carbonation of modeled recycled coarse aggregate on the mechanical properties of modeled recycled aggregate concrete. *Cem. Concr. Compos.* 89, 169–180.
- Li, B., Dai, S., Zhan, Y., Xu, J., Guo, X., Yang, Y., Chen, Y., 2022. Strength criterion of recycled aggregate concrete under triaxial compression: model calibration. *Constr. Build. Mater.* 320, 126201.
- Li, W., Guo, Y., Zhang, X., Dong, W., Li, X., Yu, T., Wang, K., 2024. Development of self-sensing ultra-high-performance concrete using hybrid carbon black and carbon nanofibers. *Cem. Concr. Compos.* 148, 105466.
- Liu, H., Zhu, X., Zhu, P., Chen, C., Wang, X., Yang, W., Zong, M., 2022. Carbonation treatment to repair the damage of repeatedly recycled coarse aggregate from recycled concrete suffering from coupling action of high stress and freeze-thaw cycles. *Constr. Build. Mater.* 349, 128688.
- Lu, W., 2019. Big data analytics to identify illegal construction waste dumping: a Hong Kong study. *Resour. Conserv. Recycl.* 141, 264–272.
- Ma, Z., Liu, M., Tang, Q., Liang, C., Duan, Z., 2020. Chloride permeability of recycled aggregate concrete under the coupling effect of freezing-thawing, elevated temperature or mechanical damage. *Constr. Build. Mater.* 237, 117648.
- Mazurana, L., Bittencourt, P., Scremin, F., Neves Junior, A., Possan, E., 2021. Determination of CO<sub>2</sub> capture in rendering mortars produced with recycled construction and demolition waste by thermogravimetry. *J. Therm. Anal. Calorim.* 1–10.
- Meng, E., Yu, Y., Yuan, J., Qiao, K., Su, Y., 2017. Triaxial compressive strength experiment study of recycled aggregate concrete after high temperatures. *Constr. Build. Mater.* 155, 542–549.

- Meng, E., Yu, Y., Zhang, X., Su, Y., 2020. Experimental and theoretical research on the mechanical performance of totally recycled concrete under triaxial compression after high temperatures. *Constr. Build. Mater.* 261, 120012.
- Recycled Aggregate for Concrete (GB/T25177-2012), 2014. China Architecture and Building Press, Beijing (in Chinese).
- Salesa, Á., Pérez-Benedicto, J.A., Colorado-Aranguren, D., López-Julián, P.L., Esteban, L. M., Sanz-Baldúz, L.J., Sáez-Hostaled, J.L., Ramis, J., Olivares, D., 2017. Physico-mechanical properties of multi-recycled concrete from precast concrete industry. *J. Clean. Prod.* 141, 248–255.
- Silva, S., Evangelista, L., De Brito, J., 2021. Durability and shrinkage performance of concrete made with coarse multi-recycled concrete aggregates. *Constr. Build. Mater.* 272, 121645.
- Specification for Mix Proportion Design of Ordinary Concrete (JGJ 55-2011), 2011. Ministry of Housing and Urban-Rural Development of the People's Republic of China (in Chinese).
- Standard for Technical Requirements and Test Method of Sand and Crushed Stone (or Gravel) for Ordinary Concrete (JGJ 52-2006), 2006. China Building Industry Press, Beijing, China (in Chinese).
- Tang, Z., Hu, Y., Tam, V.W., Li, W., 2019. Uniaxial compressive behaviors of fly ash/slag-based geopolymeric concrete with recycled aggregates. *Cem. Concr. Compos.* 104, 103375.
- Tang, Q., Ma, Z., Wu, H., Wang, W., 2020. The utilization of eco-friendly recycled powder from concrete and brick waste in new concrete: a critical review. *Cem. Concr. Compos.* 114, 103807.
- Thomas, C., De Brito, J., Gil, V., Sainz-Aja, J., Cimentada, A., 2018. Multiple recycled aggregate properties analysed by X-ray microtomography. *Constr. Build. Mater.* 166, 171–180.
- Thomas, C., De Brito, J., Cimentada, A., Sainz-Aja, J., 2020. Macro-and micro-properties of multi-recycled aggregate concrete. *J. Clean. Prod.* 245, 118843.
- Wang, S., Wang, W., Zhang, X., 2008. Calculation and analysis on energy consumption of residential buildings in severe cold region based on life cycle theory. *Build. Sci.* 04, 58–61.
- Wang, Y., Deng, Z., Xiao, J., Sheng, J., 2020. Mechanical properties of recycled aggregate concrete under multiaxial compression. *Adv. Struct. Eng.* 23 (12), 2529–2538.
- Wang, X., Li, W., Guo, Y., Kashani, A., Wang, K., Ferrara, L., Agudelo, I., 2024. Concrete 3D printing technology for sustainable construction: a review on raw material, concrete type and performance. *Dev. Built Environ.* 17, 100378.
- Wei, L., Xiao-Guang, J., Zhong-Ya, Z., 2019. Triaxial test on concrete material containing accelerators under physical sulphate attack. *Constr. Build. Mater.* 206, 641–654.
- Wu, H.J., Yuan, Z.W., Zhang, L., Bi, J., 2012. Life cycle energy consumption and CO<sub>2</sub> emission of an office building in China. *Int. J. Life Cycle Assess.* 17, 105–118.
- Wu, Y., Liu, C., Bai, G., Liu, H., Meng, Y., Wang, Z., 2023. 3D printed concrete with recycled sand: pore structures and triaxial compression properties. *Cem. Concr. Compos.* 139, 105048.
- Xiao, J., Yuan, B., Lei, B., 2007. Test and analysis of recycled coarse aggregate performance[J]. *Coal Ash China* 19 (1), 14–16.
- Xiao, J., Li, L., Shen, L., Poon, C.S., 2015. Compressive behaviour of recycled aggregate concrete under impact loading. *Cem. Concr. Res.* 71, 46–55.
- Xiao, J., Li, A., Ding, T., 2016. Life cycle assessment on CO<sub>2</sub> emission for recycled aggregate concrete. *Dongnan Daxue Xuebao (Ziran Kexue Ban)/Journal of Southeast University (Natural Science Edition)* 46 (5), 1088–1092.
- Xiao, J., Wang, C., Ding, T., Akbarnezhad, A., 2018. A recycled aggregate concrete high-rise building: structural performance and embodied carbon footprint. *J. Clean. Prod.* 199, 868–881.
- Xiao, J., Hao, L., Cao, W., Ye, T., 2022a. Influence of recycled powder derived from waste concrete on mechanical and thermal properties of foam concrete. *Journal of Building Engineering* 61, 105203.
- Xiao, J., Zhang, H., Tang, Y., Deng, Q., Wang, D., Poon, C.-S., 2022b. Fully utilizing carbonated recycled aggregates in concrete: strength, drying shrinkage and carbon emissions analysis. *J. Clean. Prod.* 377, 134520.
- Xing, W., Tam, V.W., Le, K.N., Hao, J.L., Wang, J., 2022. Life cycle assessment of recycled aggregate concrete on its environmental impacts: a critical review. *Constr. Build. Mater.* 317, 125950.
- Xu, Z., Li, J., Wu, P., Wu, C., 2021. Experimental investigation of triaxial strength of ultra-high performance concrete after exposure to elevated temperature. *Constr. Build. Mater.* 295, 123689.
- Xue, H., Zhu, H., Guo, M., Shao, S., Zhang, S., Zhang, Y., 2023. Modeling for predicting triaxial mechanical properties of recycled aggregate concrete considering the recycled aggregate replacement. *Constr. Build. Mater.* 368, 130447.
- Yang, H., Meng, S., Deng, Z., 2011. Stress-strain curves of high-performance recycled concrete under conventional triaxial compression. *Journal of Jiangsu University (Natural Science Edition)* 32 (5), 597–601.
- Yang, N., Damgaard, A., Lü, F., Shao, L.-M., Brogaard, L.K.-S., He, P.-J., 2014. Environmental impact assessment on the construction and operation of municipal solid waste sanitary landfills in developing countries: China case study. *Waste Manag.* 34 (5), 929–937.
- Yang, Y., Wu, C., Liu, Z., Zhang, H., 2022. 3D-printing ultra-high performance fiber-reinforced concrete under triaxial confining loads. *Addit. Manuf.* 50, 102568.
- Zhu, P., Zhang, X., Wu, J., Wang, X., 2016. Performance degradation of the repeated recycled aggregate concrete with 70% replacement of three-generation recycled coarse aggregate. *Journal of Wuhan University of Technology-Mater. Sci. Ed.* 31 (5), 989–995.
- Zhu, P., Hao, Y., Liu, H., Wei, D., Liu, S., Gu, L., 2019. Durability evaluation of three generations of 100% repeatedly recycled coarse aggregate concrete. *Constr. Build. Mater.* 210, 442–450.